國立台灣大學理學院物理學系

碩士論文

Department of Physics

College of Science

National Taiwan University

Master Thesis

比較不同張量網路演算法應用在二微多體量子物理系統之優劣

Comparison between Tensor Network Algorithms for Two Dimensional Infinite Quantum Many-Body Systems

周昀萱

Yun-Hsuan Chou

指導教授：高英哲博士

Advisor: Ying-Jer Kao, Ph.D.

中華民國 105 年 4 月

April, 2016


國立臺灣大學
教學勵品・愛國愛人

誌謝

隨著時光流逝，終於完成了我在物理系的碩班生涯。比起大學在材料系的無聊日子，這三年的經歷讓我感到彌足珍貴。

首先我要感謝高英哲老師的指導與包容。讓比較晚才理解並進入狀況的我也能有機會學習現在十分流行的 Tensor Network 演算法並參與開發 Uni10 的工作，讓我了解在設計 CPU 與 GPU 程式時該有的相關資訊與技巧。並在我研究十分掙扎時給予我研究的方向與建議，也讓我有許多機會與其他學者討論以克服問題，對於我的研究有了長足的幫助。

再來是要感謝組上的同學。其中特別感謝謝昀達學長在他繁忙日程裡，仍撥隴指導一個剛開始不怎麼會寫 c/c++ 的菜鳥，並讓我對 Tensor Network 相關的演算法有更進一步的認識。再來我想感謝從未謀面的張學文學長，許許多多研究上的問題, 都可以在神秘的玩貝資料夾中得到答案或起發。還要感謝感謝楊淵棨學長、吳柏寬學長、郭子傑學長、李致遠學長、高文瀚、林育平、易德、吳凱析對於我研究與課業上的種種幫助。其中特別感謝吳柏寬學長與林育平，除了對於我在物理理論、學業和娛樂上的幫忙外，也讓本應因研究卡關而在研究室崩潰的夜晚變得十分熱鬧充滿活力，並授與了我二階張亮黑魔導的頭銜。

最後，十分想感謝我的父母。不論我的選擇結果是好與壞、風險高或低，總是不斷地給與我精神上的鼓勵與物質上的支持，感謝你們的包容，才我能讓我毫無顧慮、充實的過完我碩班的時光，體驗著不一樣的人生。

摘要

如何判斷多體量子系統的相變化，且從微觀系統來得到巨觀上的物理性質，在現代仍為凝態物理學中十分有趣的領域。

從 NRG 的為起點開始，多年來出現了許多突破性的演算法。其中 DMRG 在一維的系統的模擬中得到了相當好的結果。但在二微系統中，因為 Area law 的關係使其表現不如在一微系統中精確，不僅如此，在二維系統中，計算複雜度上升之速度也非一維系統可比擬。為了解決這些問題，因而出現了許許多多不同的建立在張亮網路理論上的演算法。

此篇論文，紀錄了幾個當今較為主流或新穎並用以模疑二維量子系統的張亮網路演算法。一開始將簡單解釋張亮網路的基本理論; 再來會介紹如何實做、優化演算法，以增加精確度和降低計算複雜度。章節中也附上偽代碼，來說明實作中應注意之細節。最後會比較它們計算二維易辛模型與海森堡模型的結果，來說明各演算法之優缺點。

Abstract

Determining the phase transition of many body systems and the physical properties of macroscopic systems from microscopic description are still challenging in condense matter physics.

Since the numerical renormalization group (NRG) came out, various algorithms sprang up like mushrooms for analyzing these problems . Among all, the density matrix renormalization group (DMRG) could be considered as the most remarkable outcome, which analyze accurately in one dimensional systems. However, it perform worse in two dimensional systems. Not only the physical reasons, such as the area law, but also the rapid increment of computational complexity which is much higher than in one dimensional systems.

In order to study the phenomenals in twe-dimensional systems. First of all, we briefly introduce the tensor network theory. Secondly, we recorded some of popular tensor network algorithms which are developed for handling the problems in two-dimensional systems. Furthermore, the network diagrams and pseudo-code are presented, which gives the instruction of how to implement these algorithms.

Key words— matrix product state(MPS), projected entangled pair state(PEPS), projected entangled simplex state, infinite time-evolveing block-decimation, corner transfer matrix, tensor renormalization group, Benchmarks, uni10.

Contents

List of Figures

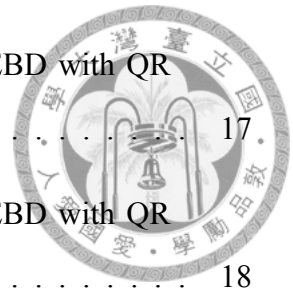

List of Tables

Chapter 1

Introduction

1.1 Overview

Understanding the phenomena of quantum many-body systems is one of the most challenging problems in condensed matter physics due to the coefficients required for describing entire systems grows exponentially with system size. For instance, If we desired to fully describe a N-site spin chain and each spin has d probable states, the requirement of coefficients is d^N. As a result, it is impossible to simulate the system whose size is larger than 50 for classical computers due to the rapid increment of computational consumptions.

Various numerical methods have been developed to address the problems mentioned above. For instance, density matrix renormalization group (DMRG) [1] [2] acquire the accuracy ground state energy and provide a dominant tool to study properties of one dimensional systems. Furthermore, the theory of DMRG is related with matrix product states (MPS) [3] [4] , which could describe the wave-function of one dimensional system and be explicitly represented by *tensor diagrams*. Therefore, DMRG is recognized as the one of the most successful method in one-dimensional systems. However, it's failure in higher dimensional systems due to the insufficiency of dealing with the entanglement in systems from matrix product states. For two-dimensional lattices, the projected entangled pair state (PEPS) [5] [6] has been applied to deal with that problem and many algorithms

sprang up like mushrooms, such as time-evolving block decimation [7] [8] and multiscale entanglement renormalization ansatz [9].

Chapter 2

Tensor Network Theory

This section begins from a fundamental question: How to draw a tensor network diagrams? In tensor network theory [10] [11] [12], we are used to represent tensors as the notations, shown in Fig. 2.1, because *tensor diagrams* can fully map to quantum states of any geometric lattice systems explicitly. Furthermore, base on its clear representation, the implementation of tensor network algorithms become simply.

2.1 Representation of tensors in tensor Networks

In mathematical concept, a tensor is considered as a multi-dimensional array of scalers. The arrangement of the elements in a tensor is dependent on its *indices* and the *rank* of a tensor is equivalent to the number of indices. Thus, a scaler (T), a vector (T_i) and a matrix (T_{ij}) can be recognized as a rank-0, rank-1 and rank-2 tensor, and so on.

Graphically, we usually use a node and few bonds to represent a tensor. Some specified examples are shown in figure 2.1, the number of bond is equal to the rank of tensor, which means that notations without bonds, with a single bond, with two bonds and with three bonds are considered as scalers, vectors, matrices and rank-3 tensors. Moreover, the dimension of a rank-N tensor D_{total} is dependent on the dimensions of the bonds in the

corresponded notions except that the dimension of a rank-0 tensor (scalers) is 1,

$$D_{total} = \begin{cases} 1 & \text{, if } N = 0 \\ \chi_1\chi_2\chi_3\cdots\chi_N & \text{, if } N \neq 0 \end{cases} \tag{2.1}$$

For instance, assume that the dimensions of the indices of the rank-3 tensor $T_{\alpha\beta\gamma}$, shown in Fig. 2.1(iv) are χ_α, χ_β and χ_γ. The tensor $T_{\alpha\beta\gamma}$ contains $\chi_\alpha\chi_\beta\chi_\gamma$ components.

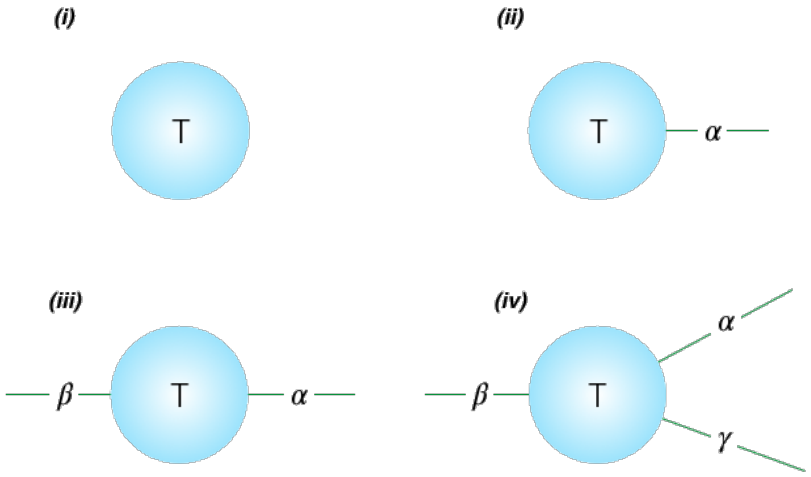

Figure 2.1: Usually we use a note and few bonds to compose a tensor and the numbers of bond depend on the rank of tensor. (i) A tensor without bonds is a scaler T, (ii) A tensor with one bond is a vector T_α, (iii) A tensor with two bonds is a Matrix $T_{\alpha\beta}$, (iv) A tensor with three bonds is a rank-3 tensor $T_{\alpha\beta\gamma}$.

2.2 Tensor operations and tensor network diagrams

In the computational languages, a fold tensor can be regard as just a container of the elements. It is not endowed with meanings until unfolded to a specified shape. In other words, we must transform it to a tensor less than rank-3 before doing any operation. The process is also called *permuteation*.

2.2.1 Permutation

See Fig. 2.2, the goal of this example is to the permute the tensor $A_{\alpha\beta\gamma}$ into $\hat{A}_{\alpha\gamma\beta}$,

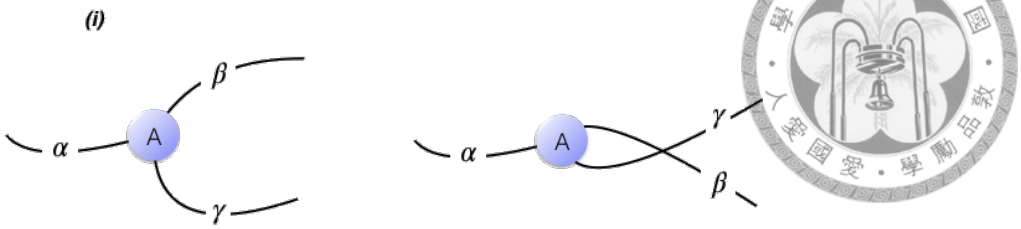

Figure 2.2: Permute tensor $A_{\alpha\beta\gamma}$ to $\hat{A}_{\alpha\gamma\beta}$

$$A_{\alpha\beta\gamma} \rightarrow \hat{A}_{\alpha\gamma\beta} \tag{2.2}$$

Nevertheless, the arrangements of tensor $A_{\alpha\beta\gamma}$ is modified to $\hat{A}_{\alpha\gamma\beta}$. The components of them are exact equivalence.

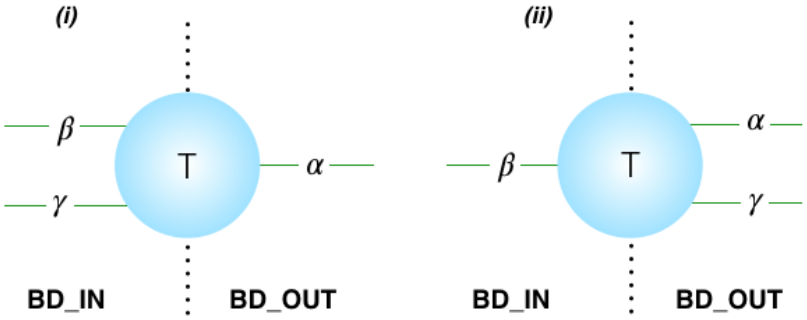

Figure 2.3: (i) Unfold a tensor to a matrix $T_{\chi_\beta\chi_\gamma,\chi_\alpha}$, (ii) Unfold a tensor to a matrix $T_{\chi_\beta,\chi_\alpha\chi_\gamma}$.

In order to explain more clearly, we separate the tensor to two part, incoming (BD_IN) and outgoing (BD_OUT) which are also designed for distinguishing different types of *uni10::Bond* in *Uni10 Library* [], to show what the meaning of reshape is in the linear algebra. The total dimensions of the bonds in the part BD_IN and BD_OUT corresponds to rows and columns of a matrix. For instance, if the indices of $T_{\alpha\beta\gamma}$ ordered like Fig. 2.3(i), $T_{\alpha\beta\gamma}$ is equivalent to a matrix $M_{\chi_\beta\chi_\gamma,\chi_\alpha}$, where χ_α, χ_β and χ_γ are the dimensions of the bonds, α, β and γ. Similarity, The tensor shown as Fig. 2.3(ii) can be recognized as a matrix $M_{\chi_\beta,\chi_\alpha\chi_\gamma}$.

2.2.2 Tensor contraction

Tensor contraction is defined as the sum of all products of the shared indices of tensors. For instance, the tensor diagram of contracting two rank-2 tensors $A_{\alpha\beta}$ and $B_{\beta\gamma}$ is shown as Fig. 2.4 which can be written as,

$$C_{\alpha\gamma} = \sum_{\beta=1}^{\chi_\beta} A_{\alpha\beta} B_{\beta\gamma}, \tag{2.3}$$

and obviously this example corresponds to the inner-product of two matrices $A_{\chi_\alpha,\chi_\beta}$ and $B_{\chi_\beta,\chi_\gamma}$,

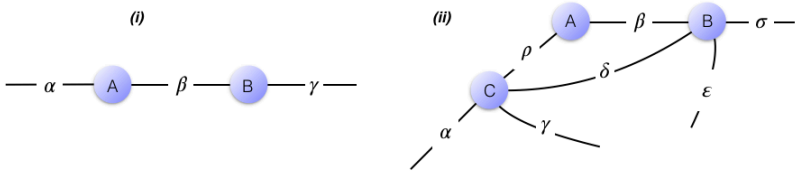

Figure 2.4: (i) Contract rank-2 tensors $A_{\alpha\beta}$ and $B_{\beta\gamma}$ (ii) Contract a rank-2 tensor $A_{\rho\beta}$, and two rank-4 tensors $B_{\sigma\varepsilon\delta}$ and $C_{\delta\rho\alpha}$

Now that we considered a more complicated example shown in Fig2.4(ii). The equation of the tensor diagram is described as,

$$D_{\alpha\gamma\sigma\epsilon} = \sum_{\beta\rho\delta} A_{\rho\beta} B_{\beta\sigma\epsilon\delta} C_{\gamma\delta\rho\alpha}, \tag{2.4}$$

In order to contract the tensors $A_{\rho\beta}$, $B_{\beta\sigma\epsilon\delta}$ and $C_{\gamma\delta\rho\alpha}$ in the diagram, we can follow the steps, see Fig. 2.5

1. Selected the pair of tensors arbitrarily: In this example, we choose the tensor $A_{\rho\beta}$ and $C_{\gamma\alpha\delta\rho}$ firstly.

2. Permute the tensors to specified shape and operate the inner-product: As shown in Fig. 2.5(ii)-(iii) Reshape (unfold) $A_{\rho\beta}$ and $C_{\gamma\alpha\delta}$ to matrices A_{χ_ρ,χ_β} and $C_{\chi_\gamma\chi_\alpha\chi_\delta\chi_\rho}$

and do the inner-product,

$$\theta_{\gamma\alpha\delta\beta} = C_{\chi_\gamma\chi_\alpha\chi_\delta\chi_\rho}\dot{A}_{\chi_\rho,\chi_\beta} \tag{2.5}$$

3. Repeat the step (1) and (2) until all tensors be contracted: See Fig. 2.5(iii)-(iv), repeat the steps again to contract the remained tensors $\theta_{\gamma\alpha\delta\beta}$ and $B_{\beta\sigma\delta\varepsilon}$

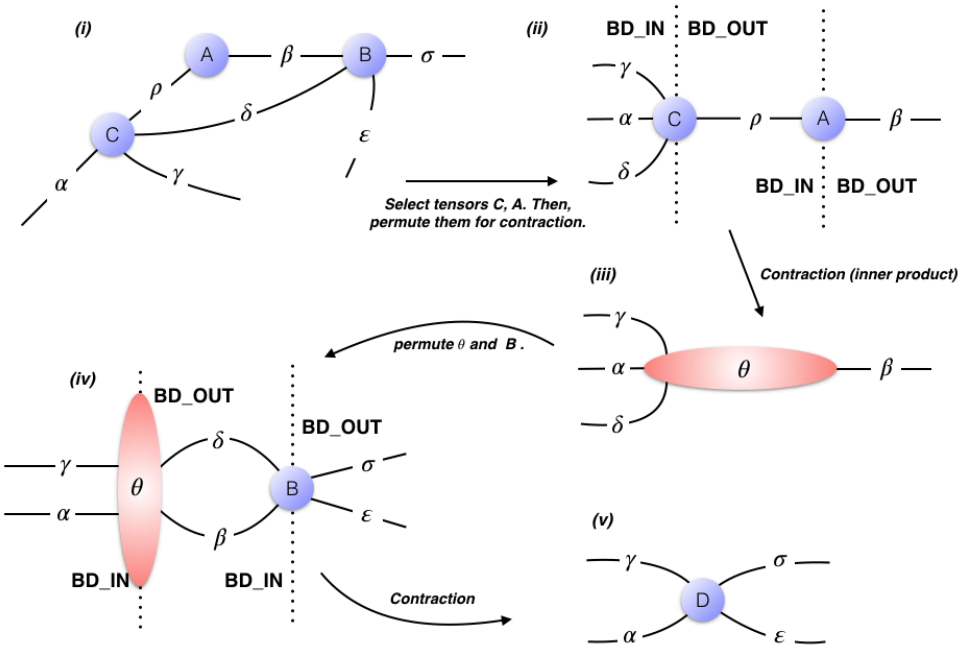

Figure 2.5: The contraction procedures of the network shown in Fig2.4

Actually, the choice in step(1) is restricted in some algorithms, because the order of the network contraction is strongly correlated to the efficiency, such as the corner transfer matrix, the fast full update and so on. For example, if the dimensions of the bonds of the tensors, $A_{\rho\beta}$, $B_{\beta\sigma\epsilon\delta}$ and $C_{\gamma\delta\rho\alpha}$ [Fig. 2.5(i)], are D. The consumption of the contraction of $A_{\rho\beta}$ and $C_{\gamma\delta\rho\alpha}$ is D^4. However, it increase to D^6, if we contract $B_{\beta\sigma\epsilon\delta}$ and $C_{\gamma\delta\rho\alpha}$ at first. Therefor, how to find the cheapest contraction order is a non-trivial issue. Nevertheless, it still hard be determined efficiently when the network contains too many tensors.

2.3 Describe Quantum states with tensor network

Before drawing a many-body system with tensor-network representation, we should discuss how to describe a many-body systems which is a chain of N particles, with each particles having d states. The system can be regard as a congregation of N localized particles and we have studied that a pure state corresponds to a vector in Hilbert space. Hence, the wave-function of many-body systems can be described by N subspace,

$$|\Psi_N\rangle = \sum_{i_1,i_2,\ldots,i_N} C_{i_1,i_2,i_3,\ldots,i_N} |i_1\rangle \otimes |i_2\rangle \otimes \ldots \otimes |i_N\rangle, \tag{2.6}$$

where each individual $|i_1\rangle, |i_2\rangle, \ldots, |i_N\rangle$ spanned by an orthogonal basis which the degree of freedom is d. After writing down the formulation of the wave function, eq.2.6, we are able to build a tensor-network representation for quantum states. The wave function $|Psi_N\rangle$ is shown as Fig. 2.6(a), each bond of the tensor corresponds to the local Hilbert space $|i_n\rangle$ and the dimension of each bond is equivalent to the probable states of the particle on the nth site and the coefficients of the rank-N tensor corresponds to $C_{i_1,i_2,i_3,\ldots,i_N}$.

No matter from eq. 2.6 or Fig. 2.6(a), we can directly notice that the number of coefficients, $C_{i_1,i_2,i_3,\ldots,N}$, is proportional to d^N. Therefor, it is impossible to fully describe a many-body system by a classical machine, if the system size larger then fifty. Fortunately, according to the theory of MPS [], the wave-function can be decomposed to two subsystem by Schmidt decomposition and there are more details in chapter.3.

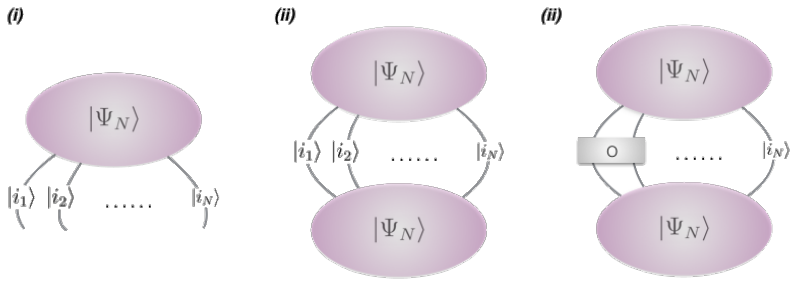

Figure 2.6: (i) Wave-function: $|\Psi_N\rangle$ (ii) Norm of $|\Psi_N\rangle$; $\langle\Psi_N \mid \Psi_N\rangle$ (iii) Expectation value of observable O; $\langle\Psi_N| O |\Psi_N\rangle$

Chapter 3

2-D Imaginary Time Evolving Block Decimation

In this chapter we introduce some different ways to implement two-dimensional imaginary time-evolving block decimation and apply them in calculation of ground state of Heisenberg and transverse Ising model on two-dimensional square lattice. In section 3.1 and 3.2, we briefly review the idea of imaginary time evolution (TEBD) [7] [8] and explain how to extend it to an infinite two-dimensional system [13]. Second, we briefly review another implementation which is able to make 2D-iTEBD more stable[14]. In the last section 3.4, we record various particulars which are helpful optimizing algorithms.

3.1 Imaginary Time Evolution

Theoretically, if having the imaginary time evolution operator $e^{-\tau H}$, we could project any random states to the ground state, as long as the wave-function can be written as,

$$|\psi_0\rangle = \frac{e^{\tau H}|\Psi\rangle}{\| e^{\tau H}|\Psi\rangle \|} \tag{3.1}$$

but according to the eq.3.1, we may found that the number of coefficients in an origin evolution operator $e^{-\tau H}$ is proportional to $2^N \times 2^N$. On the other words, it is impossible

to update entire system directly. In order to restricting the rapid dimensional growth, we apply *Suzuki Trotter decomposition* to approximate. The main idea of *Suzuki Trotter* is decomposing the whole system to lots of units cell and using some smaller operations to update the wave-function.

$$e^{\delta A+B} = e^{\delta A}e^{\delta B} + O(\delta^2) \tag{3.2}$$

eq.3.2 means the first-order Suzuki Trotter decomposition, and A and B are non-commutative with each other.

Now that the dimension of the evolution operator is reduced to a n-site operator and in chapter **??**, we have shown that a many-body system can map to a MPS [3][4] or PEPS [5] structure, so we can draw the process of updating a ground state like Fig.3.1,

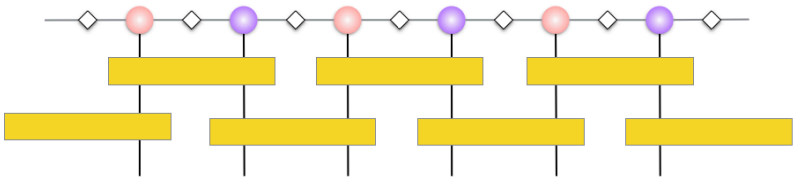

Figure 3.1: The red and blue tensor denotes on *odd* and *even* sites. The yellow one are time evolution operators $e^{-\tau H_{k,k+1}}$, $e^{-\tau H_{k+1,k}}$

On the other work, contract the tensors in Fig.3.1 repeatedly until the ground state energy to the minimum. The remained tensor is considered as the ground state of the system. So the next question: How can we contract them and preserve the structure like Fig3.2? This answer is iTEBD.

Figure 3.2: The simple form of a matrix product state.

3.2 Simple Infinite Imaginary-Time Evolving Block Decimation for 2-D system

In this section, we apply the TN diagrams to introduce various implementation methods. More theoretical details are included in the references [15] [16] [17].

3.2.1 Simple Description of iTEBD for 1-D system

The algorithm start from 2 random states and 2 random diagonal matrices which are considered as entanglement between particles. In the TN diagrams, Fig.3.3, the states and entanglement between neighbor sites are represented by the nodes and bonds with different colors.

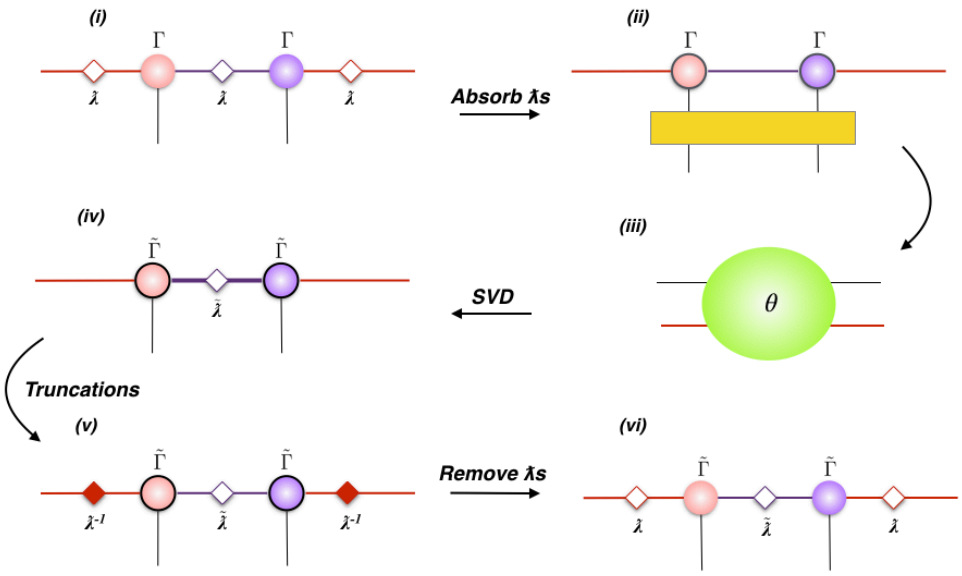

Figure 3.3: (i)Absorb all λ to Γ. (ii) Contract an evolution operator $e^{-\delta H}$ for evolving the system. (iii) Decompose the tensor θ by SVD. (iv) Truncate and Update the states and λ on the green bond.(v) Remove λ for obtaining the states. (iv) After updating the states and λ on the purple bond, apply the way to update the red bond and repeat all the steps until the ground state convergence.

The processes shown in Fig.3.3 is a standard strategy for implementation of iTEBD and also called *Simple Update*.

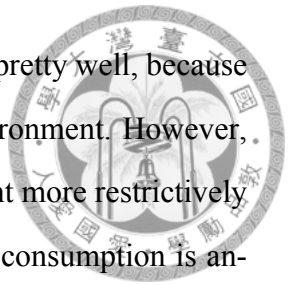

In one dimensional system, the performance of Simple Update is pretty well, because 1-D systems obey the canonical form and have less influences of environment. However, in 2-D systems, due to the area law, we need consider the environment more restrictively when measuring the local observable. Moreover, the computational consumption is another serious problem, owing to the growth of a state's dimension which is proportional to dD^4.

In order to solving that obstacles, optimizations of 2-D algorithms became an important part in condense matter physics. This chapter we focus on obtaining good enough projected entangled pair states from 2-D iTEBD and the strategies of improving measurement would be shown in following chapters.

3.2.2 Description and Pseudocode of iTEBD for 2-D system

Now that we stated to extend it to a two dimensional system. In chapter.**??**, we have known that a two dimensional many-body system is able to be represented by PEPS. Due to impossibly drawing an network of infinite sites, the structure of infinite PEPS (iPEPS) is decided by the geometry of the lattice and the unit cell we chosen. In usual, the size of unit cell depend on the n-site evolution operator. For instance, if the target is updating iPEPS of a square lattice with 2-site operator, the tensor diagram would be drawn as Fig.3.4.

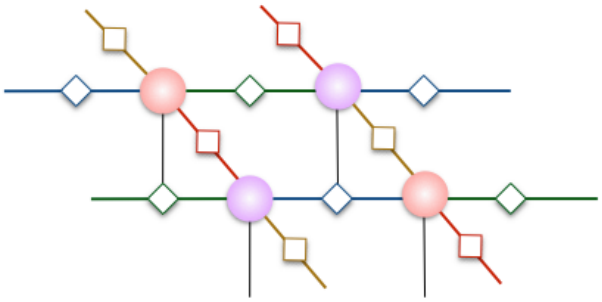

Figure 3.4: Four sites unit cell in iPEPS.

After setting the form of iPEPS, we start to deal the question of updating states. The most intuitive scheme is to apply the scheme of *Simple Update* which is shown in Fig.3.5.

The steps are similar to the iTEBD on 1-D systems. However, there are some differences. Firstly, the projected entangled pair states is a rank-5 tensor. Secondly, there are more entangled should be considered, due to increased neighbor sites.

More theoretical descriptions are written in [**??**][**??**]. Here, we explain the methods with TNs and some simple pseudocodes. The basic idea of *2-D iTEBD* is to update the states from four directions by *Simple Update*. The example starting from updating the green bond is shown in Fig.3.5 and Fig.3.6,

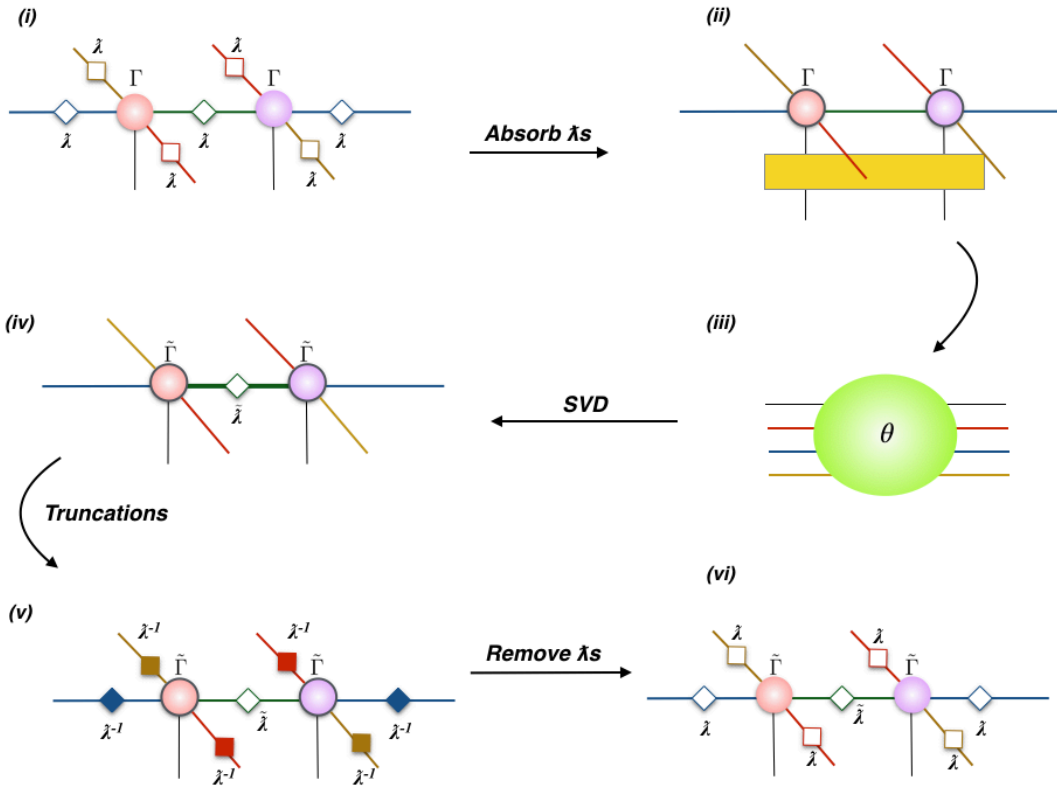

Figure 3.5: Absorb all λ to Γ. (ii) Contract an evolution operator $e^{-\delta H}$ for evolving the system. (iii) Decompose the tensor θ by SVD. (iv) Truncate and Update the states and λ on the green bond.(v) Remove λ for obtaining the states. (iv) Obtain a original form of iPEPS. Repeat all the step to update the other bonds until the ground state energy convergence

It's the same as one dimensional case, The first step is to absorb all λ around the sites. The tensor with gray bold means the state have absorbed all entanglements. Secondly, contract the gate, $e^{-\delta H}$, for getting the tensor θ. Thirdly, apply singular value decomposition to update states and the entanglement on the green bond. After decomposing θ, we found that the dimension of the green bond increase to dD^4. Therefor, truncation plays

a significant roles for keeping the dimension in the algorithm. In the end of the updating processes, multiply pseudo inverse of all λ to the tensors for reducing to original form.

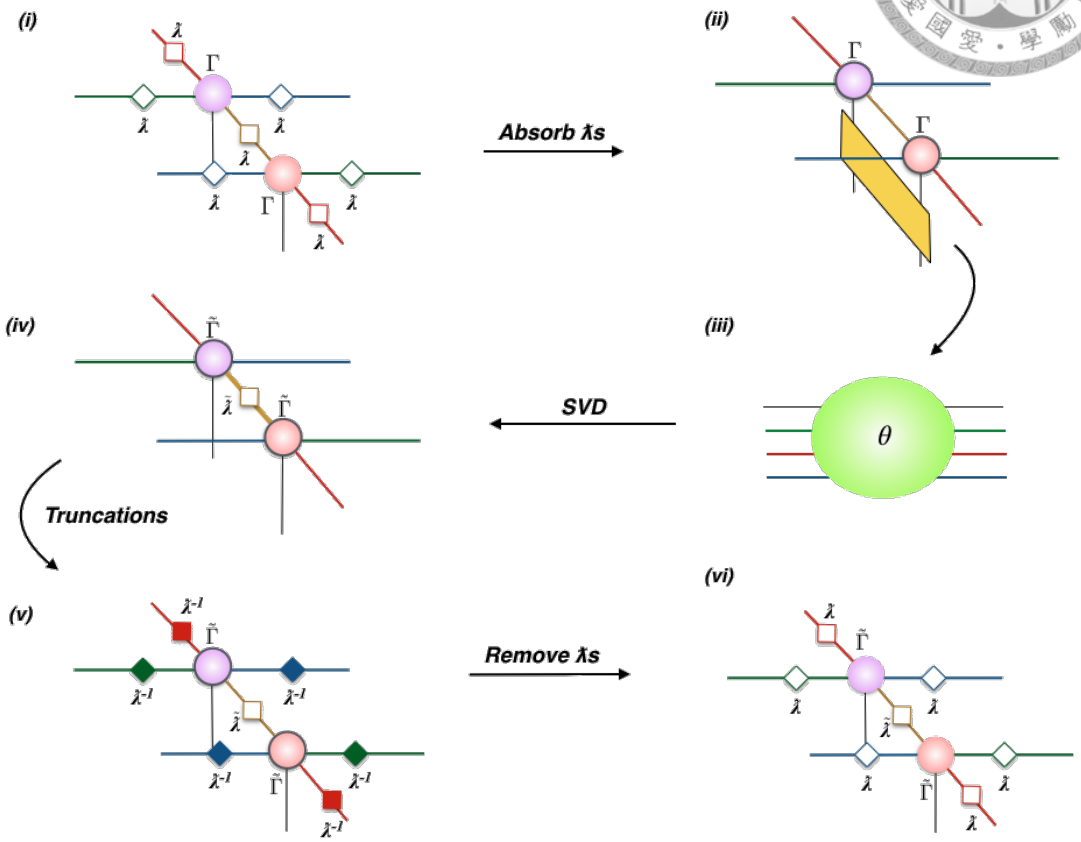

Figure 3.6: Update the yellow bond and the steps are similar to Fig.3.5

For easily to imagine how to updating the others directions. The updating steps of yellow bond are shown In Fig.3.6.

3.3 Ameliorate two-dimensional iTEBD

This method which make the algorithm more stable was published by *M. B. Hastings* [14]. Although *Simple Update* shown in section.3.2.2 can obtain pretty good states, it's not stable and efficient enough. The reason is that too many multiplications of pseudo inverse λ at the step Fig.3.5(v). In numerical methods, it's hard to deal the problem of dividing the value which is equal or approach to zero. On the other words, the more inverse operations, the more the probability of bring about divergence or destroying algorithms.

For reducing the risk of breaking algorithms. Firstly, declare the states Γ which include two entanglements among them. For instance, In Fig.3.7(i), the red tensor is considered as multiplication of A and the λ on the yellow. The purple one is multiplication of B and remained λ. Secondly, in Fig.3.7(ii), because the entanglements on red and blue bonds are included in tensor B, we just need absorb the yellow one and contract the evolution operation for obtaining tensor C. Thirdly, we contract the red and blue λ to the red and blue bonds which belong to the original tensor A in tensor C for getting θ. Fourthly, getting the $\tilde{B}$ from decomposing and truncating θ. Owing to avoid multiplying inverse matrices, we get $\tilde{A}$ by contracting tensor C and $\tilde{B}$ and multiply an inverse λ of yellow bond for removing the entanglement and reducing to original form.

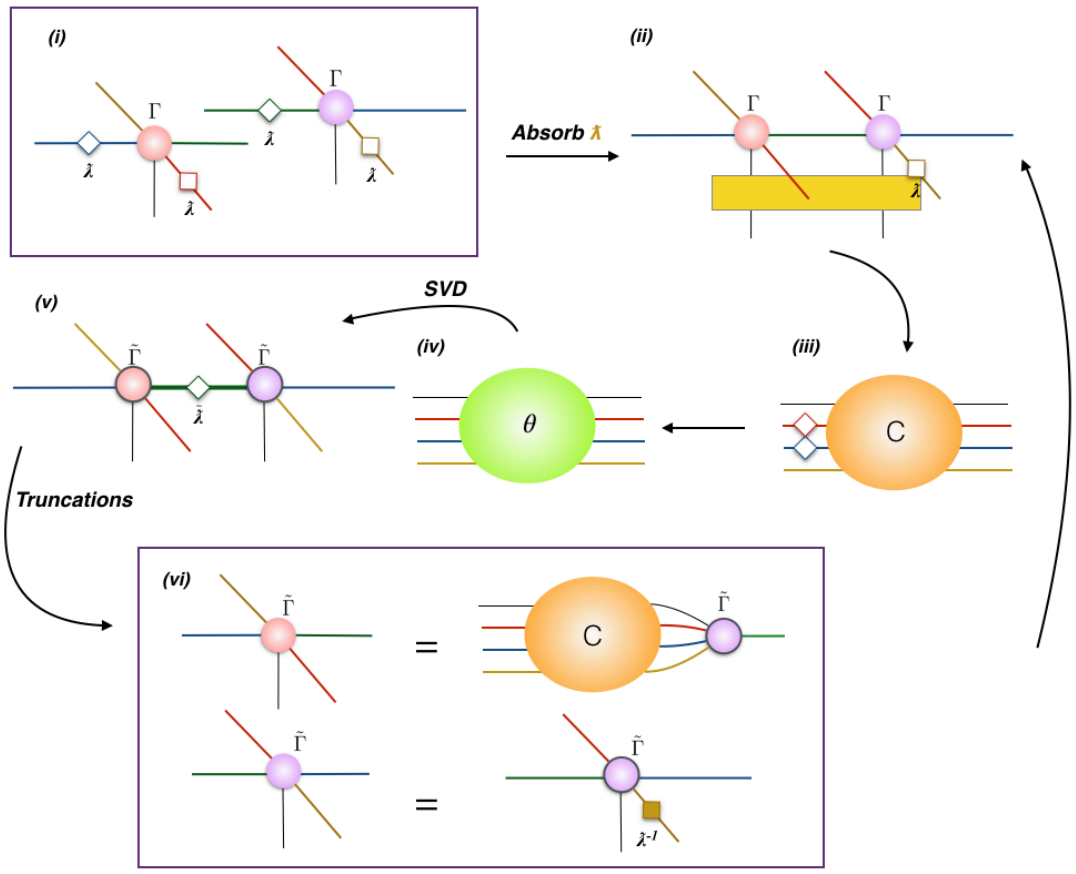

Figure 3.7: The tensor network diagrams for the ameliorated 2-D iTEBD.

Finally, repeat all the processes shown in Fig.3.7 to update different bonds until the convergence of the ground state energy.

3.4 Optimizations

3.4.1 Initialization

Intuitively, the initialization of states should not affect the result. However, it's a serious misunderstanding. Actually, stating from a awful initial sates may break the algorithms or hardly converge.

From the viewpoint of physics, translational invariance is one of essential properties in many-body system, So we can assume that the group state on two sites should be similar. For instance, if the TN diagram of the states is shown as Fig 3.8(i), Fig 3.8(ii) might be the better way to initialize the states.

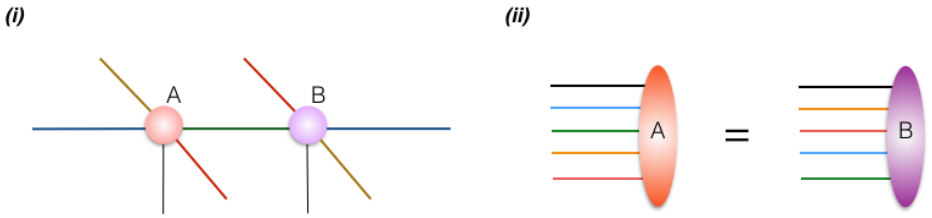

Figure 3.8: (i) The structure of PEPS, (ii) The initialization of states

3.4.2 Truncation Error

3.4.3 QR decomposition

Though the strategy described in previous sections improve the stability, it's not efficient enough. The reason why is that the dimension of tensor θ, in Fig.3.5(iii) and Fig.3.7(iii), is proportional to d^2D^6. In addition to that, the time complexity of singular value decomposition is proportional to $O(NM^2)$. In conclusion, those steps are expensive and the dimension of tensor θ must be redued for accelerating.

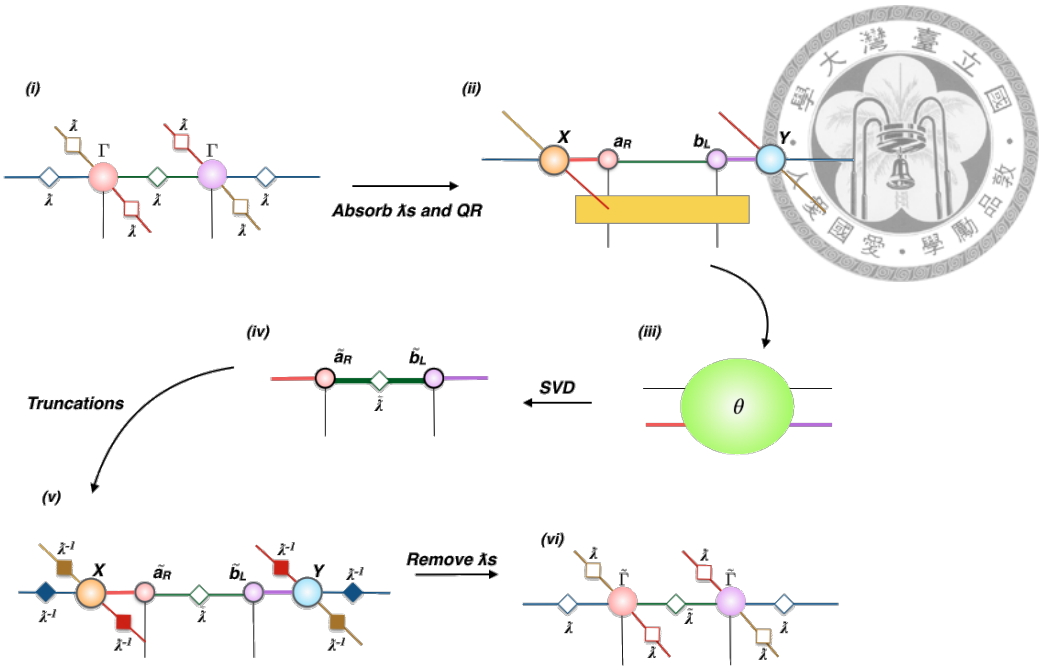

Figure 3.9: The tensor network diagrams for the ameliorated 2-D iTEBD.

To achieve the goal, the projected pair state must be decomposed by QR decomposition [13] [**?**]. The processes making *Simple Update* more efficient is illustrated in Fig 3.9. Most of the steps shown in Fig 3.9 are like in Fig 3.5. The only difference is that after absorbing all the λ, we decompose the state to an orthogonal matrix and an upper triangular matrix by QR. For instance, in Fig 3.9 (ii), the state A is decomposed to an orthogonal matrix X and upper triangular matrix a_R. Due to the columns of X are orthonormal, $XX^\dagger$ is equal to I. In the other word, the tensor X can be ignored and we just need consider the tensor a_R by QR. Similarity, the state B can be decomposed to a lower triangular b_L and an orthogonal matrix Y by LQ which is equivalence to operate QR decomposition after transpose the matrix. Next, (iii) we can obtain the tensor θ whose dimension is d^2D from a_R, b_L and an evolution operator.

The strategy to accelerate *Ameliorate Simple Update* is shown in the Fig 3.10 and its main idea is also to reduce the dimension of θ.

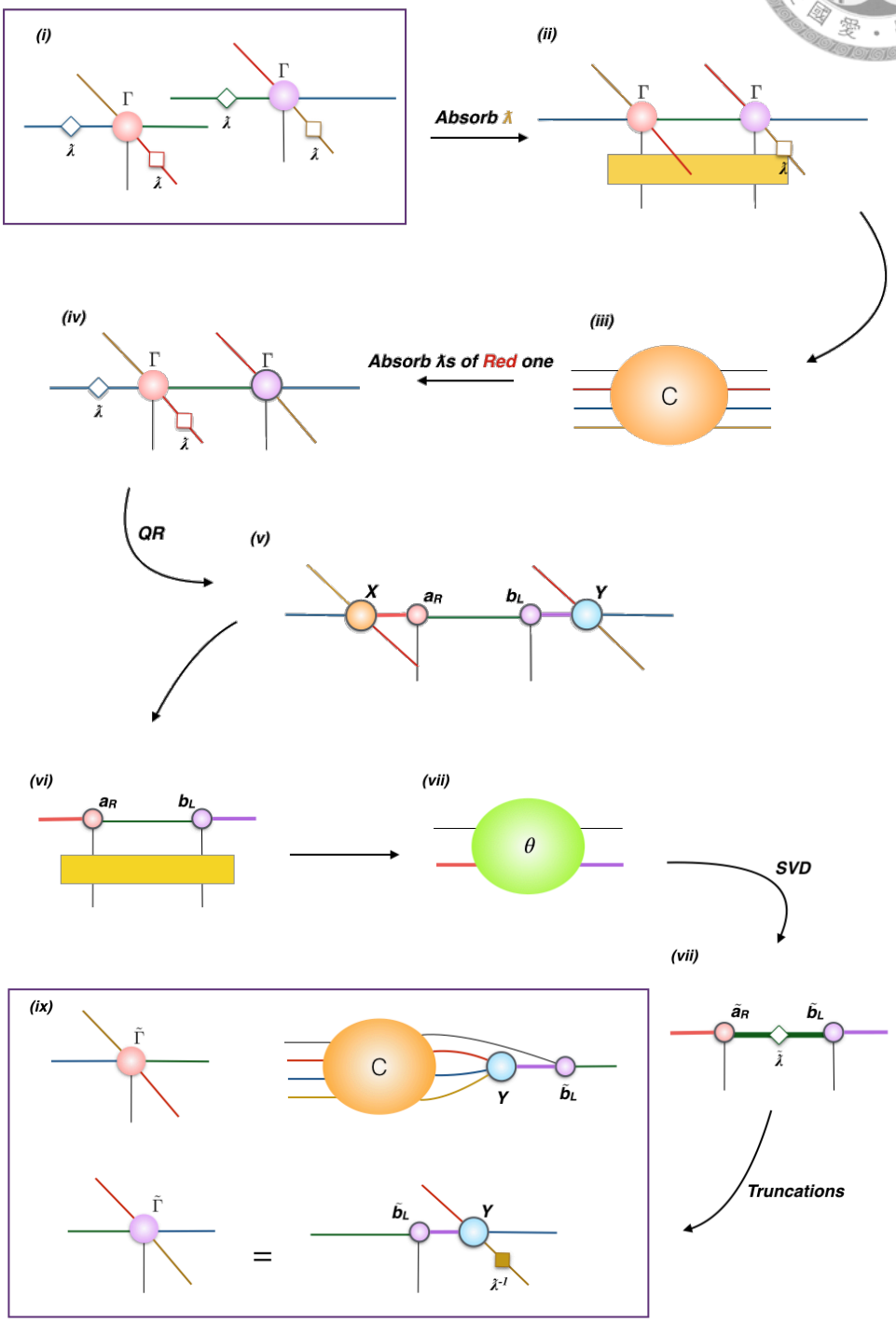

Figure 3.10: The tensor network diagrams for the ameliorated 2-D iTEBD.

3.5 Comparison

So far, we have benchmarked the improved iTEBD.

3.5.1 Different Initializations

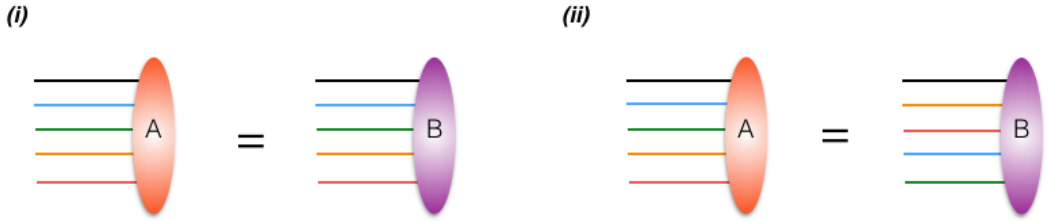

Figure 3.11: (i) Type 1, (ii) Type 2

See Fig 3.12, the both cases are

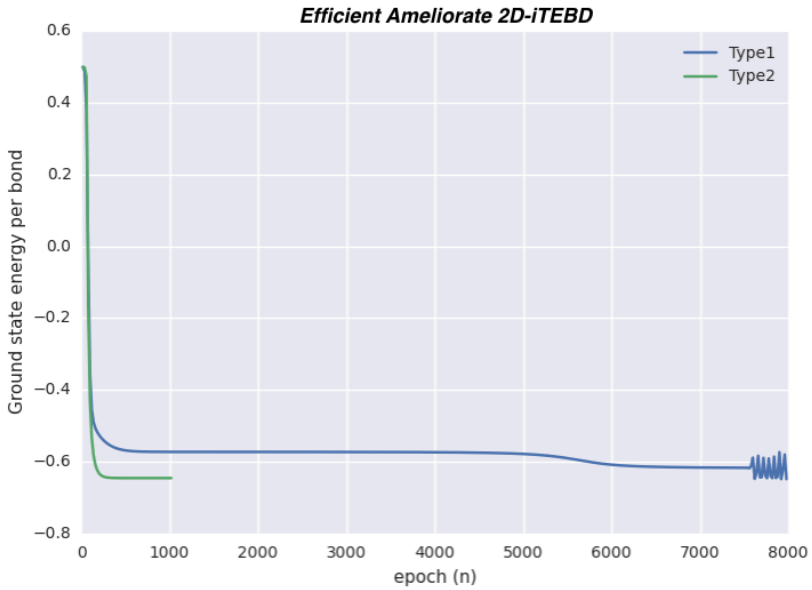

Figure 3.12: The Blue line represents updating tensors from the initial state shown in Fig 3.11 (i) and the green one represents updating from Fig 3.11 (ii)

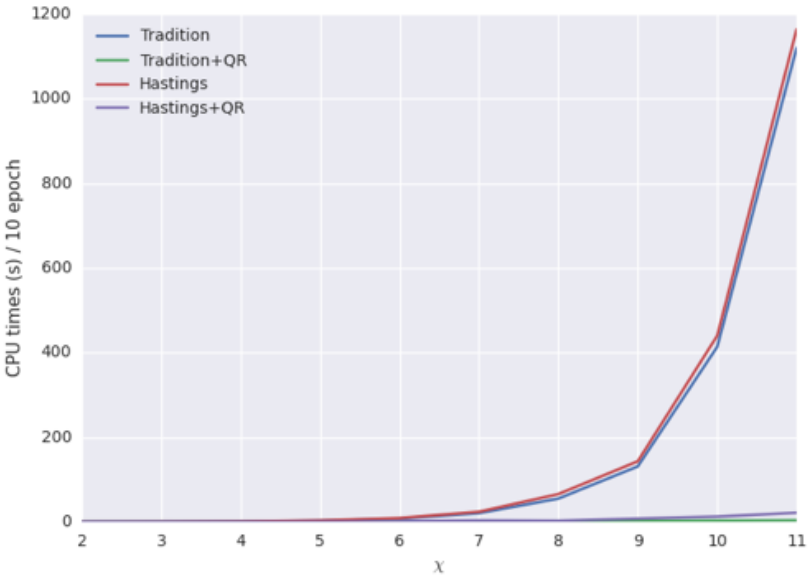

Figure 3.13

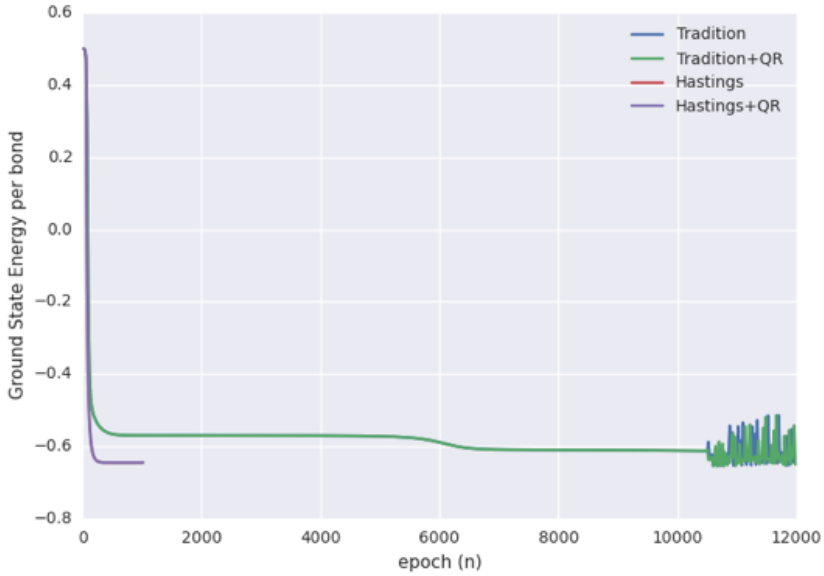

Figure 3.14

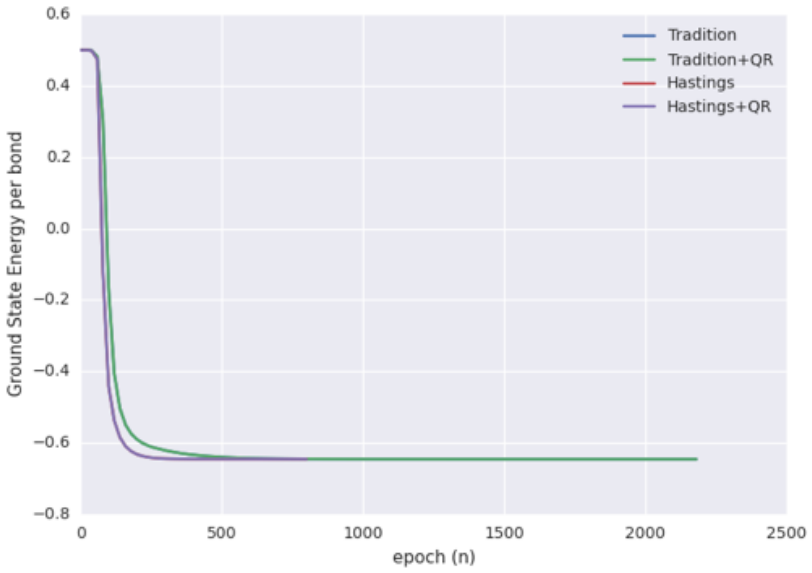

Figure 3.15

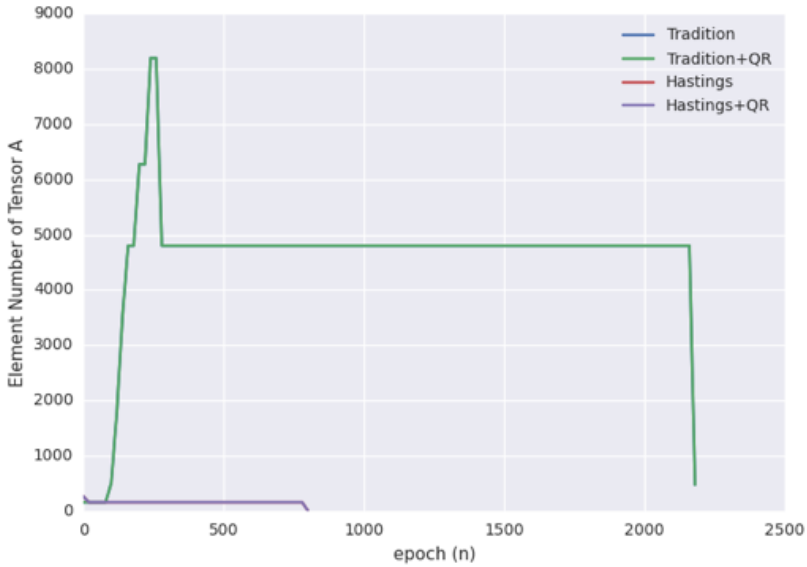

Figure 3.16

Chapter 4

Infinite Projected Entangled Simplex State

4.1 Simplex-solid State

The simplex-solid state of an SU(N) quantum anti-ferromagnet was derived by Arovas [] and the most significant conclusion is that any simplex states could be described by a natural generalization of the AKLT [] valence bond solid state which means that the bond signlets of the AKLT could be extended to N-site simplices.

The concept of simplex-solid states ansatz were introduce by Xie et al []. The tensor-network representation of simplex states is called projected entangled simplex state (PESS) which is also considered as an extension of PEPS [] obeying the area law of entanglement entropy and characterizing any states if the dimension of the virtual bonds are large enough. The difference from the PEPS is that the entanglement among the virtual particles is described by entangled simplex tensors which depend on the structure of PESS. For example, in Fig. 4.1(b) there are three virtual particles within the simplex state, so the entangled simplex tensor S_{mnl} is a rank-3 tensor.

For illustrating how to write down the formulation of the PESS wave function, we

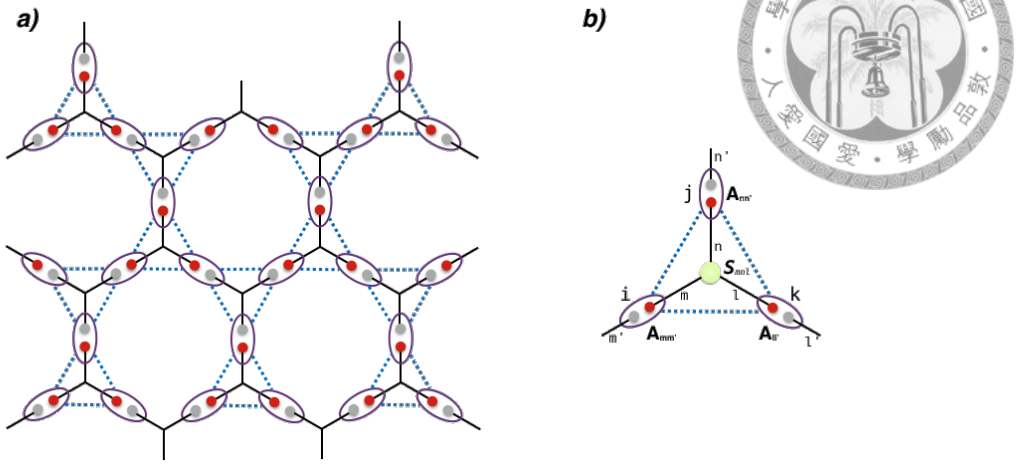

Figure 4.1: The red and blue tensor denotes on *odd* and *even* sites. The yellow one are time evolution operators $e^{-\tau H_{k,k+1}}$, $e^{-\tau H_{k+1,k}}$

begin from a simple system, the spin-2 simplex state on an infinite Kagome lattice []. See Fig. 4.1(a) each physical $S = 2$ states on the lattices could be treated as a symmetric superposition of two virtual $S = 1$ spins. According to the theory of AKLT, each neighbor simplices (triangles) share a single site symmetrically which also means that the $S = 1$ spins could be assigned to one of the simplices (vertex-sharing). Hence, there are three $S = 1$ spins in each simplex states. From the features of the $SU(2)$ group, the decomposition of the direct-product of three integer spins is written as,

$$n \otimes n \otimes n = [a_0 \times 0] \oplus \cdots \oplus [a_k \times k] \oplus \cdots \oplus [a_{3n} \times 3n] \tag{4.1}$$

$$a_k = \begin{cases} 2k+1 & , k \leq n \\ 3n+1-k & , k > n \end{cases} \quad , k = 0, 1, \ldots, 3n, \tag{4.2}$$

where a_k is a constant and k express the kth irreducible representation. Now that we can write down the product of the spins in the simplex as,

$$\underline{1} \otimes \underline{1} \otimes \underline{1} = \underline{0} \oplus (3 \times \underline{1}) \oplus (2 \times \underline{2}) \oplus \underline{3}, \tag{4.3}$$

and show that there is an unique spin-singlet state. The result encourage us to define a

virtual singlet on simplex,

$$|\psi_\alpha\rangle = \frac{1}{\sqrt{6}} \sum_{\{s_i s_j s_k\}} S^\alpha_{s_i s_j s_k} \left|s_i, s_j, s_k\right\rangle, \tag{4.4}$$

where s_i, s_j, s_k are $S = 1$ virtual spins located at site i, j and k containing in the simplex α and $S^\alpha_{s_i s_j s_k}$ is the Levi-Civita antisymmetric tensor ε_{ijk} [Fig. 4.1(b)]. For mapping the two virtual $S = 1$ spins to the spin-2 subspace, we defined the projection operator P_i on each site,

$$P = \sum_{s_i, s_i'} \sum_{\sigma_i} A^{\sigma_i}_{s_i, s_i'} \left|\sigma_i\right\rangle \left\langle s_i, s_i'\right| \tag{4.5}$$

where $|\sigma_i\rangle$ is a basis of the $S = 2$ spin at site i. $A^{\sigma_i}_{s_i, s_i'}$ is a projected matrix whose components are filled by the Clebsch-Gordan coefficients,

$$\begin{aligned}
&A^2_{11} = A^{-2}_{33} = 1, \\
&A^1_{12} = A^1_{21} = A^{-1}_{23} = A^{-1}_{32} = \frac{1}{\sqrt{2}}, \\
&A^0_{13} = A^0_{31} = \frac{1}{\sqrt{6}}, \\
&A^0_{22} = \frac{2}{\sqrt{6}},
\end{aligned}$$

Now that we can write down the wave function of the simplex-solid state,

$$|\Phi\rangle = \bigoplus_i P_i \prod_\alpha |\psi_\alpha\rangle \tag{4.6}$$

$$= \mathrm{Tr}\left(\ldots S^\alpha_{s_i s_j s_k} A^{\sigma_i}_{s_i, s_i'} A^{\sigma_j}_{s_j, s_j'} A^{\sigma_k}_{s_k, s_k'} \ldots \right) \left| \ldots \sigma_i \sigma_j \sigma_k \ldots \right\rangle . \tag{4.7}$$

and apply the tensor-network representation to descrbe it, see in Fig. 4.1(b). This structure could be extended to any higher integer spins. In conlusion, a physical $S = 2n$ (even-integer) spin is considered as a symmetric superposition of two virtual $S = n$ spins and $S = 2n - 1$ (odd-integer) is regarded as a symmetric superposition of a virtual $S = n - 1$ spin and a virtual $S = n$ spin [Fig. 4.1(a)]. More details are included in reference [] [].

4.2 Variational PESS ansatz

In this section, we will employ the formulation of the PESS wave function as a variational ansatz. The PESS ansatz is similar to the imaginary time evolution discussed in chapter.3. However, unlike the PEPS algorithms, we apply a higher rank tensor S to describe the entanglement entropy among virtual particles in a simplex state. Due to the difference, we use *high-order singular value decomposition* (HOSVD) rather than SVD to decompose wave function.

4.2.1 High-order singular value decomposition

In the section, we will introduce to Nth-order singular value decomposition (HOSVD) which is proposed for decomposing rank-N tensors and show the pseudocode to illustrate the scheme of the implementation.

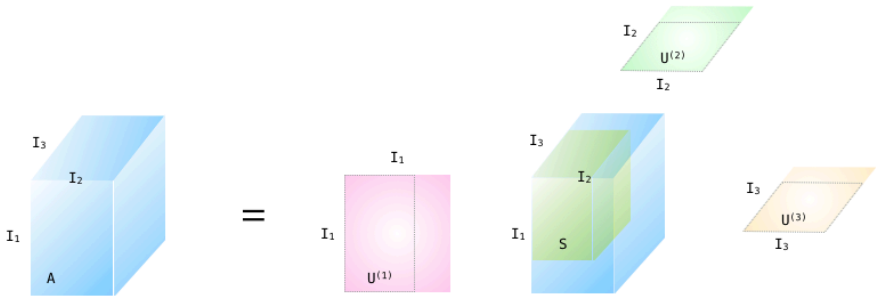

Figure 4.2: The picture of HOSVD for a rank-3 tensor A. $U^{(1)}$,$U^{(2)}$ and $U^{(3)}$ are unitary matrices and S (yellow cuboid) is a core tensor.

According to the theorem of HOSVD [], every *complex* $(I_1 \times I_2 \times \cdots \times I_N)$-tensor A could be decompose to a *core tensor* S and other n-mode unitary matrix $U^{(n)}$, where the maximum of n must be smaller than N,

$$A = S \times U^{(1)} \times U^{(2)} \times \cdots \times U^{(n)} \tag{4.8}$$

As shown in Fig. 4.2, a rank-3 tensor A is decomposed to a core tensor S (yellow cuboid)

and three unitary matrices obtaining from three different modes. The core tensor S is a *complex* $(I_1 \times I_2 \times \cdots \times I_N)$-tensor and have some significant properties,

1. Row-orthogonal: Two subtensors $S_\alpha^{(n)}$ and $S_\beta^{(n)}$ are orthogonal when $\alpha \neq \beta$.

$$\left\langle S_\alpha^{(n)}, S_\beta^{(n)} \right\rangle \quad \text{, if} \quad \alpha = \beta \tag{4.9}$$

   In other words, no matter the shape of S, each rows are orthogonal.

2. Ordering: The Frobenius-norms $\left\| S_i^{(n)} \right\|$ is ordered from large to small.

$$\left\| S_1^{(n)} \right\| \geq \left\| S_2^{(n)} \right\| \geq \cdots \geq \left\| S_{I_n}^{(n)} \right\| \geq 0, \tag{4.10}$$

   for all possible values of n.

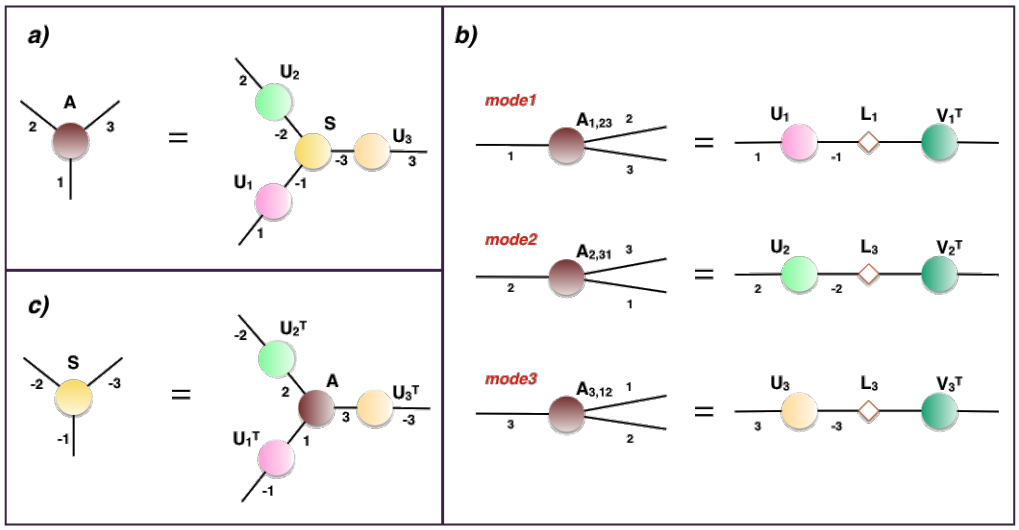

Figure 4.3: (a) Decompose A to a core tensor S and n-mode unitary matrix $U^{(n)}$, (b) Obtain tensors $U^{(n)}$ from decomposing various modes of tensor A by SVD, (c) Obtain the core tensor S from contracting all transpose unitary tensors $U^{(n)T}$

Now that we show the tensor-network representation for explaining more explicitly. If the target is to decompse a rank-3 $(N = 3)$ tensor A by 3 $(n = 3)$ modes, see in Fig .4.3(a), we can implement is by the following steps,

1. Reshaping the tensors to each modes and obtain $U^{(n)}$ by SVD , as shown in Fig. 4.3(b).

2. Contract all $U^{(n)T}$ tensors for getting S express more mathematically,

$$S = A \times U^{(1)T} \times U^{(2)T} \times \cdots \times U^{(n)T} \tag{4.11}$$

, see Fig. 4.3(c).

4.2.2 Simple update for PESS

In chapter.3, we have introduced an efficient approximation, the "simple update", for determining the PEPS wave function. In principle, the wave function of PESS can be approached by the same way. In PEPS structure, the ground-state wave function is approximated by iterated application of imaginary-time evolution operators $U(\tau) = e^{-\tau H}$ on an random PEPS state $|\Psi_t\rangle$, where τ is a small constant, see Fig. 3.1. Base on the scheme, we can obtain the ground-state wave function of PESS by following steps,

1. Split Hamiltonian H,

$$H = H_\alpha + H_\beta \tag{4.12}$$

   where α and β are dependent on the geometry of the PESS structure.

2. Obtain the evolution operator $U(\tau)$ by Trotter-Suzuki decomposition.

$$e^{-\tau H} = e^{-\tau H_\alpha} e^{-\tau H_\beta} + O(\tau^2). \tag{4.13}$$

3. Absorb the environment bond vectors, which are considered as the entanglement between each simplex states, into projection tensors, and contract all projection tensors in the simplex state with the core tensor to obtain a cluster tensor.

4. Apply the evolution operator U to the cluster tensor for obtaining a new cluster tensor.

5. Decompose the new cluster tensor by HOSVD.

6. Truncate all the projection tensors and the core tensor.

7. Absorb the inverse bond vectors for removing the entanglement on the projection tensors.

which is similar to simple update of PEPS. In the following subsections, we applied various cases to explain it more explicitly.

4.3 Infinite Kagome lattice

In the previous section, we have briefly introduced to the procedures of PESS ansatz. The first step is to choose an suitable n-PESS structure, where n is the number of projection tensors in a simplex, to split the Hamiltonian and describe the system. There are many various graphical representation for the Kagome lattice [Fig. 4.1(a)], such as 3-PESS, 5-PESS and 9-PESS, shown in ref. []. In this section, we will discuss more details about 3-PESS and 5-PESS.

4.3.1 3-PESS

In the 3-PESS case, the PESS state can be drawn as the Fig. 4.4(a), which pictures that the many-body states can be described by composing two different simplices, upward- and downward-oriented triangular as shown in Fig 4.4(b). Each simplices contain three rank-3 projection tensors, $A^{\sigma_i}_{mm'}$ $A^{\sigma_j}_{nn'}$ and $A^{\sigma_k}_{ll'}$ and a rank-3 core tensor, S^{α}_{mnl} or $S^{\beta}_{m'n'l'}$. Therefore, the form of the Hamiltonian is re-written by eq. 4.12,

$$H = H_\alpha + H_\beta \quad \text{, where} \quad H_\alpha = H_\Delta, \quad H_\beta = H_\nabla \tag{4.14}$$

Next, utilize the imaginary-time evolution operator $e^{-\tau H}$ to an random initial state $|\Psi_0\rangle$ iteratively. According to the theorem of Trotter-Suzuki decomposition, the evolution operator can be decomposed into two product terms, when $\tau \to 0$. Hence, the evolution

operator operator of 3-PESS can be written as,

$$e^{-\tau H} = e^{-\tau H_{\Delta}} e^{-\tau H_{\nabla}} + O(\tau^2) \tag{4.15}$$

when the value of τ is small enough.

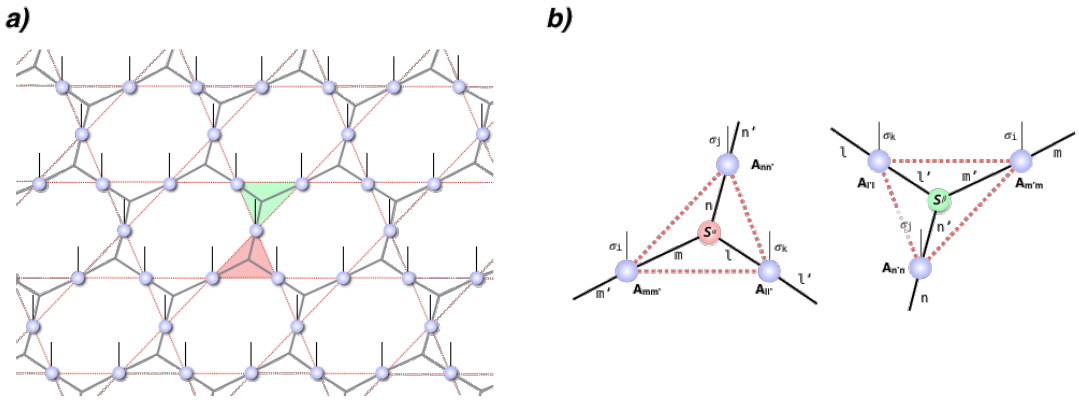

Figure 4.4: The graphical representation of 3-PESS. (a) The PESS state can be considered as composed by two simplices, upward- (green triangular) and downward-triangular (green triangular). The red dash-line represent as the geometry of the kagome lattice. As this figure shown, the projection tensors (Blue circle) are rank-3 with the dimension dD^2, where d is the dimension of the physical basis and D is the dimension of the virtual bonds (gray line), and the entangled simplex tensors, with the dimension D^3, are located at the cross of three virtual bonds (gray line) in each simplex states. (b) Two simplices in 3-PESS structure. These two type simplices, clustered with the sharing projection tensors, $A^{\sigma_i}_{mm'}$, $A^{\sigma_j}_{nn'}$ and $A^{\sigma_k}_{ll'}$. However, their entangled simplex tensor are individual. In (a), the core tensor of the red simplex is S^{α}_{mnl} and the green one is $S^{\beta}_{m'n'l'}$

After determining the evolution operators, $e^{\tau H_{\Delta}}$ and $e^{\tau H_{\nabla}}$, we apply the schem of the simple update to approximate theground state wave function of 3-PESS. As shown in Fig. 4.6, we take an example of updating upward-triangular simplex α to illustrate,

1. Obtain a clustered simplex tensor θ: Firstly, absorb all the environment bond vectors surrounding the simplex state. See Fig. 4.5(a), the environment vectors, $\lambda^{\beta}_{m'm}$, $\lambda^{\beta}_{n'n}$ and $\lambda^{\beta}_{l'l}$, are obtained from the entangled simplex tensor of simplex β, due to the

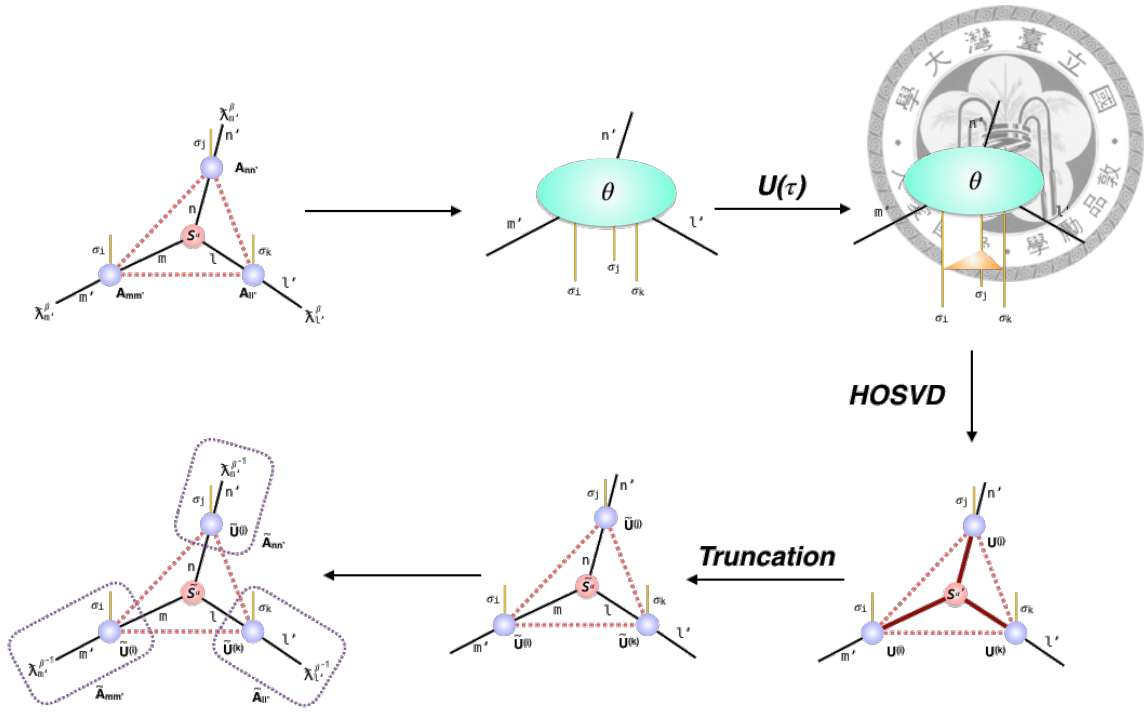

Figure 4.5: The schem of the simple update for 3-PESS. The more detail descriptions are in the paragraph

canonical form of the PESS [],

$$\sum_{n,l} S^{(\beta)}_{mnl}\left(S^{(\beta)}_{m'nl}\right) = \delta_{m,m'}\lambda^{(\beta)2}_{m} \tag{4.16}$$

$$\sum_{l,m} S^{(\beta)}_{mnl}\left(S^{(\beta)}_{mn'l}\right) = \delta_{n,n'}\lambda^{(\beta)2}_{n} \tag{4.17}$$

$$\sum_{m,n} S^{(\beta)}_{mnl}\left(S^{(\beta)}_{mnl'}\right) = \delta_{l,l'}\lambda^{(\beta)2}_{l} \tag{4.18}$$

and base on the features of HOSVD, shown in eq. **??**. The λs can be simply obtained, when we decompose the clustered tensors of the simplex β in the updating process. Secondly, contract all tensors in simplex state to obtain the clustered tensor θ. The mathematical representation of the step is written as,

$$\theta^{\sigma_i\sigma_j\sigma_k}_{m'n'l'} = \sum_{mnl,m'n'l'} S^{(\alpha)}_{mnl}\lambda^{(\beta)}_{m''}A^{\sigma_i}_{mm'}\lambda^{(\beta)}_{n''}A^{\sigma_j}_{nn'}\lambda^{(\beta)}_{l''}A^{\sigma_k}_{ll'} \tag{4.19}$$

2. Apply the evolution operator $U(\tau)$: In eq. 4.15, we have generated the evolution operator for 3-PESS ansatz. Due to updating upward-triangles simplex, $U(\tau)$ is

defined as,

$$U(\tau) = e^{-\tau H_{\Delta}} \tag{4.20}$$

Now that, we utilize $U(\tau)$ to the cluster tensor θ, see Fig. 4.5(c) and obtain a new cluster tensor θ',

3. Decompose θ' into the general form of the simplex state: Apply the high-order singular value decomposition (HOSVD) to obtain new projection tensors, $U^{(\sigma_i)}$, $U^{(\sigma_j)}$ and $U^{(\sigma_k)}$, and a new core tensor of simplex α, $S^{(\alpha)'}$, see Fig. 4.5(d). During operating HOSVD, we need save the environment bond vectors, $\lambda_m^{(\alpha)}$, $\lambda_n^{(\alpha)}$ and $\lambda_l^{(\alpha)}$, surrounding the simplex β. All $\lambda^{(\alpha)}$ could be obtained from decomposing different modes of θ'. As shown in Fig. 4.3(b).

4. Truncation: In order to avoid the exponential increment of the virtual bonds dimension, we need truncate the brown bonds in Fig. 4.5(d) to specified dimension D' which can be fixed to original dimension D or determined dynamically by setting an truncation error as the discussion in section 3.4.2. The simple way is to truncate projection tensors firstly,

$$U^{\sigma_i} \rightarrow \widetilde{U}^{\sigma_i}_{mm'} \tag{4.21}$$

$$U^{\sigma_j} \rightarrow \widetilde{U}^{\sigma_j}_{nn'} \tag{4.22}$$

$$U^{\sigma_k} \rightarrow \widetilde{U}^{\sigma_k}_{ll'} \tag{4.23}$$

Next, contract the transpose of these tensors with θ', as Fig. 4.3(c), to obtain $\widetilde{S}^{\alpha}$ in Fig. 4.5(e), where

$$\widetilde{S}^{(\alpha)} = \sum_{m'n'l'} \theta'^{\sigma_i\sigma_j\sigma_k}_{m'n'l'} \widetilde{U}^{\sigma_i}_{mm'} \widetilde{U}^{\sigma_j}_{nn'} \widetilde{U}^{\sigma_k}_{ll'} \tag{4.24}$$

5. Absorb the inverse environment bond vectors $\lambda^{(\beta)^{-1}}$ into truncated projection tensors: To obtain the updated projection tensors $\widetilde{A}^{\sigma_i}_{mm'}$, $\widetilde{A}^{\sigma_j}_{nn'}$ and $\widetilde{A}^{\sigma_k}_{ll'}$, we need remove

the influence of environment,

$$\widetilde{A}^{\sigma_i}_{mm'} = \sum_{m''} \lambda^{(\beta)}_{m'm''} \widetilde{U}^{\sigma_i}_{mm''} \tag{4.25}$$

$$\widetilde{A}^{\sigma_j}_{nn'} = \sum_{n''} \lambda^{(\beta)}_{n'n''} \widetilde{U}^{\sigma_j}_{nn''} \tag{4.26}$$

$$\widetilde{A}^{\sigma_k}_{ll'} = \sum_{l''} \lambda^{(\beta)}_{l'l''} \widetilde{U}^{\sigma_i}_{ll''} \tag{4.27}$$

see Fig. 4.5(f),

At here, one updated epoch is completed. Finally, the ground state will be obtained by iterating the procedures for each simplex, upward- and downward- triangular (Δ, ∇), until the wave function of PESS converge,

4.3.2 5-PESS

In the 5-PESS structure [Fig. 4.6(a)], the procedure to approximate the ground state wave function is similar to 3-PESS. However, due to the transformation of the structure, the simplices should be re-defined. In the 5-PESS ansatz, each simplex state is composed by an upward- and a downward-triangular and the most significant change is that the core tensors are located on the physical sites. As shown in Fig. 4.6(b), each simpliices contain 4 projection tensors $A^{\sigma_i}_{ii'}$ $A^{\sigma_j}_{jj'}$ $A^{\sigma_k}_{kk'}$ and $A^{\sigma_l}_{ll'}$, and a core tensor, $S^{\sigma_s(\alpha)}_{ijkl}$ or $S^{\sigma_s(\beta)}_{i'j'k'l'}$. Therefor, we can split the Hamiltonian into

$$H = H_\alpha + H_\beta \quad \text{,where} \quad H_\alpha = H_{\textcolor{red}{\boxtimes}}, H_\beta = H_{\textcolor{green}{\boxtimes}} \tag{4.28}$$

and as previous section, the evolution operator is written as,

$$e^{-\tau H} = e^{-\tau H_{\textcolor{red}{\boxtimes}}} e^{-\tau H_{\textcolor{green}{\boxtimes}}} + O(\tau^2) \tag{4.29}$$

when $\tau \to 0$.

Next, apply the simple update scheme as Fig. 4.7. Most of steps are similar to 3-PESS,

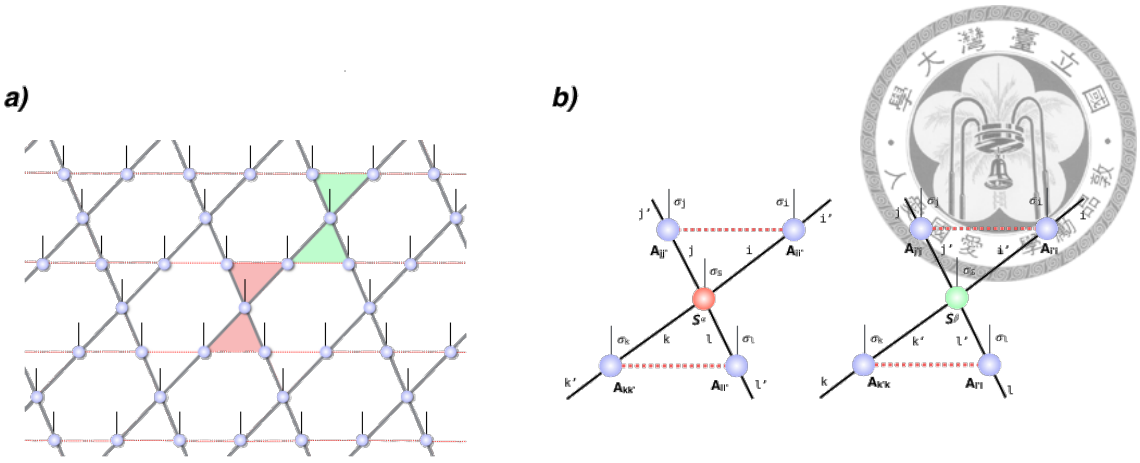

Figure 4.6: The graphical representation of 3-PESS. (a) The PESS state can be considered as composed by two simplices, upward- (green triangular) and downward-triangular (green triangular). The red dash-line represent as the geometry of the kagome lattice. As this figure shown, the projection tensors (Blue circle) are rank-3 with the dimension dD^2, where d is the dimension of the physicla basis and D is the dimension of the virtual bonds (gray line), and the entangled simplex tensors, with the dimension D^3, are located at the cross of three virtual bonds (gray line) in each simplex states. (b) Two simplices in 3-PESS structure. These two type simplices, clustered with the sharing projection tensors, $A^{\sigma_i}_{mm'}$, $A^{\sigma_j}_{nn'}$ and $A^{\sigma_k}_{ll'}$. However, their entangled simplex tensor are individual. In (a), the core tensor of the red simplex is S^{α}_{mnl} and the green one is $S^{\beta}_{m'n'l'}$

shown as Fig. 4.5. However, we should carefully decompose the cluster tensor θ', where

$$\theta' = \theta \times U(\tau) \tag{4.30}$$

see Fig. 4.7(d). In this structure, the core tensors contain physical basis states, which means that it can't be decompose by the simply way shown in Fig. 4.3, due to

$$N \mod n \neq 0 \tag{4.31}$$

where N is the rank of the tensor θ' and n is the mode number of HOSVD. Hence, the bond σ_s, belonging to the core tensor $S^{(\alpha)}_{i'j'k'l'}$ in tensor θ', must be fixed during the decomposition. The more detail and general form of the HOSVD are written in the documentation of *Uni10 Library* [], which is implemented by c/c++ and helpful for calculating the high-rank linear algebra problems.

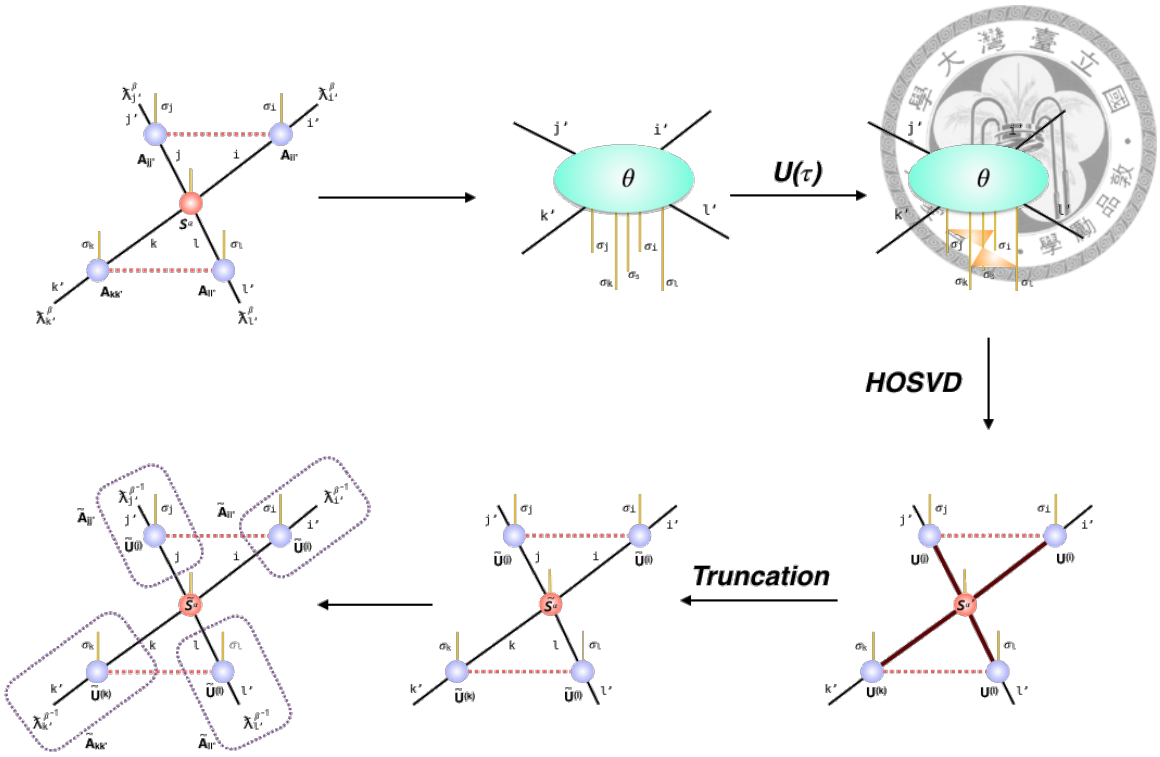

Figure 4.7: The schem of the simple update for 5-PESS. The more detail descriptions are in the paragraph

4.4 Infinite Square lattice

In previous sec. 4.3, we have verified the results in ref. [] []. In order to test and recognize the properties of the PESS ansatz more explicitly, we extend it to simulate infinite square systems and compare it with methods discussed in chap. 3.

4.4.1 4-PESS (Rank-3 projection tensors)

The 4-PESS structure could be build by two different methods, which is drawn in the ref. []. In this section, we use the concept, shown in Fig. 4.8(a), to complete the implementation.

See Fig. 4.8(a), the many-body state can be regarded as composed by two different simplices, shown in Fig. 4.8(b), repeatedly. The components of each simplices are similar to 5-PESS, but the difference is that the core tensors, $S^{(\alpha)}_{ijkl}$ and $S^{(\beta)}_{i'j'k'l'}$, are not located on

the lattice sites. Hence, the Hamiltonian is split into,

$$H = H_\alpha + H_\beta \quad \text{, where} \quad H_\alpha = H_{\square}, \quad H_\beta = H_{\square} \tag{4.32}$$

where $\square$ and $\square$ are represented simplex α and β, shown in Fig. 4.8(b). Therefor, the evolution operator can be written as,

$$e^{-\tau H} = e^{-\tau H_{\square}} e^{-\tau H_{\square}} + O(\tau^2) \tag{4.33}$$

when τ is a small constant $\to 0$.

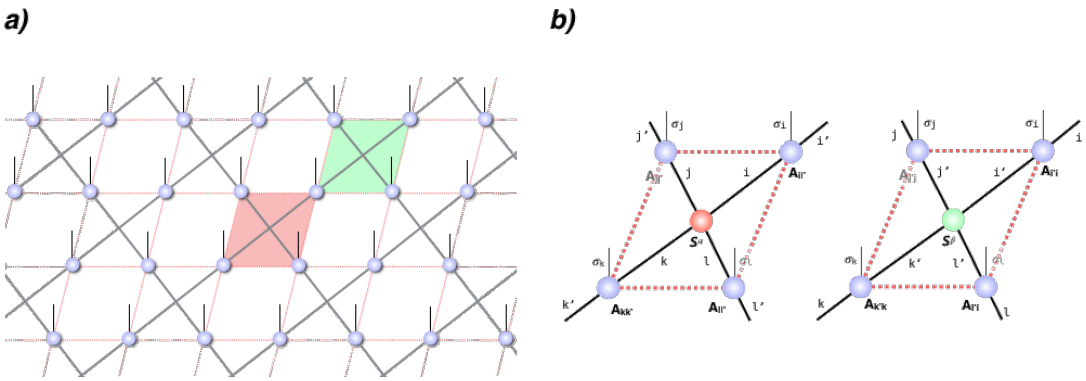

Figure 4.8: The graphical representation of 3-PESS. (a) The PESS state can be considered as composed by two simplices, upward- (green triangular) and downward-triangular (green triangular). The red dash-line represent as the geometry of the kagome lattice. As this figure shown, the projection tensors (Blue circle) are rank-3 with the dimension dD^2, where d is the dimension of the physicla basis and D is the dimension of the virtual bonds (gray line), and the entangled simplex tensors, with the dimension D^3, are located at the cross of three virtual bonds (gray line) in each simplex states. (b) Two simplices in 3-PESS structure. These two type simplices, clustered with the sharing projection tensors, $A^{\sigma_i}_{mm'}$, $A^{\sigma_j}_{nn'}$ and $A^{\sigma_k}_{ll'}$. However, their entangled simplex tensor are individual. In (a), the core tensor of the red simplex is S^{α}_{mnl} and the green one is $S^{\beta}_{m'n'l'}$

Finally, the ground state wave function can be obtained by repeating the following steps, shown in Fig. 4.9, on the simplices, α and β ($\square$, $\square$), until the wave function of PESS converge.

Before we do more restrict comparisons, it is obvious that the control of dimensional increment in the 4-PESS is better than in the PEPS [Fig. 3.4], In 4-PESS structure, the projection tensors are described by rank-3 tensors whose dimension is dD^2. However,

in the PEPS representation, the dimension of local tensors is dD^4. The reduction of tensors dimension is helpful for calculating and studying with a significant larger dimension. Nevertheless, it doesn't also mean that the 4-PESS algorithm is more efficient than PEPS one and actually it encounter in some problems when approximating the environment. We will show mare details in following sections.

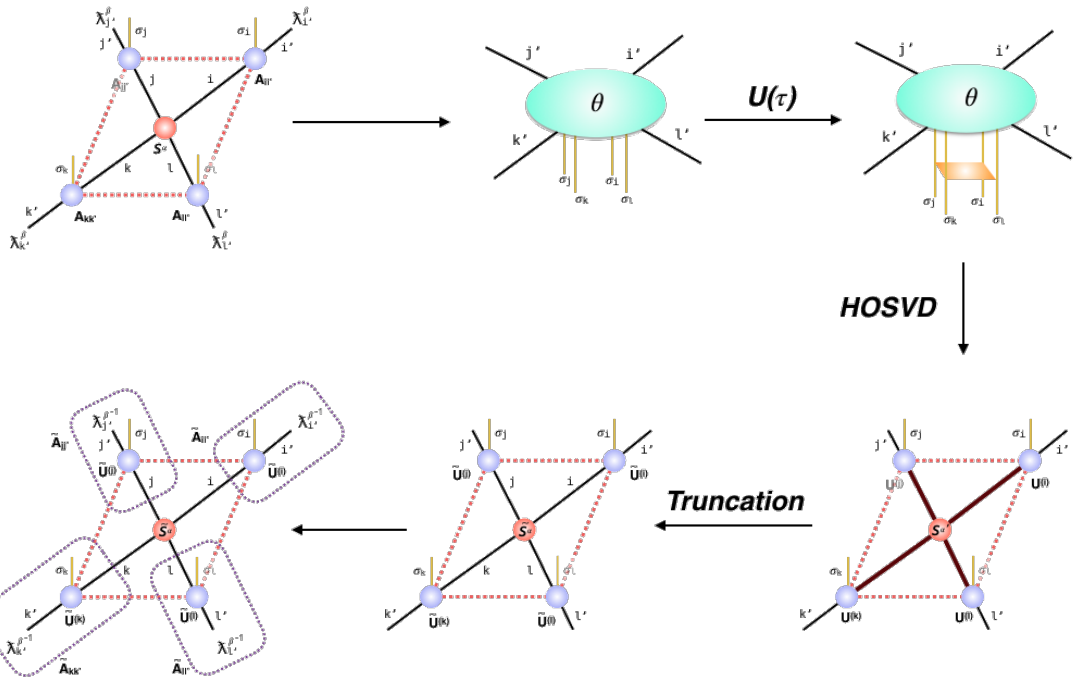

Figure 4.9: The scheme of the simple update for 4-PESS, composed by rank-3 projection tensors. The more detail descriptions are in the paragraph

Chapter 5

Corner Transfer Matrix

The *cerner transfer matrix renormalization group* (CTMRG) [] is an algorithm to numerically compute the *effective environments* which is an approximation of the environment of systems. For example, if the infinite PEPS is composed by a single tensor A^h_{uldr} repeatedly, where h express a physical basis of $\mathbb{V}$ with dimension d, and u, l, d, r are virtual bonds with dimension D, see Fig. 5.1(a). Then we can represent the scale norm $\langle\psi \mid \psi\rangle$ by a simple two dimensional tensor network ε which is characterized by reduced tensors a, shown in Fig. 5.1(b). The reduced tensor a is defined as eq.5.2,

$$a \equiv \sum_{h=1}^{d} A_h \otimes A_h^* \tag{5.1}$$

The environment $\varepsilon^{[\vec{r}]}$ of the site $\vec{r}$ could be described by the reduced tensors in the gray rectangles in Fig.5.1(c) and the *effective environments* $G^{[\vec{r}]}$ shown in Fig. 5.1(d) is target of the CTMRG.

In the following subsections, we will show more details of implementation of CTM and compare some features between obtaining the states from iPEPE and PESS.

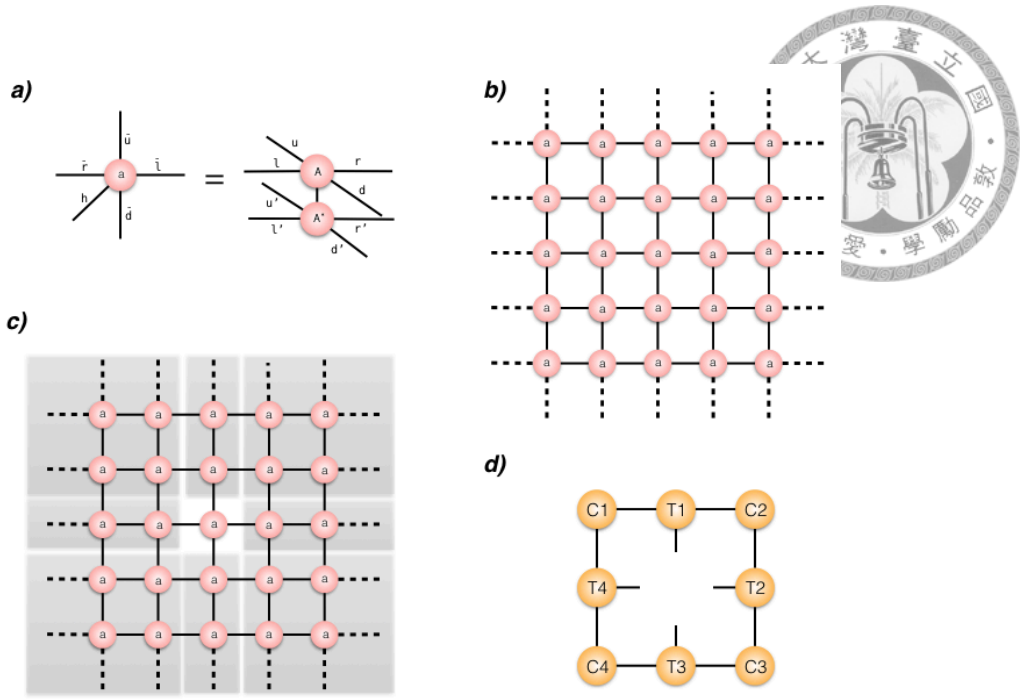

Figure 5.1: The red and blue tensor denotes on *odd* and *even* sites. The yellow one are time evolution operators $e^{-\tau H_{k,k+1}}$, $e^{-\tau H_{k+1,k}}$

5.1 Obtain States from PEPS

In chapter.3, we have discussed about obtaining the infinite PEPS state $|\psi\rangle$ of an infinite 2D square lattice by imaginary time evolution and known that the infinite PEPS could be characterized by two tensors A^h_{uldr} and B^h_{drul} repeatedly (Fig. 5.2(a)). The scaler norm of the iPEPS $\langle\psi\,|\,\psi\rangle$ is composed by reduced tensors $a_{\bar{u}\bar{l}\bar{d}\bar{r}}$ and $b_{\bar{d}\bar{r}\bar{u}\bar{l}}$(Fig. 5.2(b)), where

$$\bar{a} \equiv \sum_{h=1}^{d} A_h \otimes A_h^* \tag{5.2}$$

$$\bar{b} \equiv \sum_{h=1}^{d} B_h \otimes B_h^* \tag{5.3}$$

Then, we can consider the environment $\varepsilon^{[\vec{r_1},\vec{r_2},\vec{r_3},\vec{r_4}]}$ of a four-site structure (Fig. 5.2(c)), and try to approximate it with effective environment $G^{[\vec{r_1},\vec{r_2},\vec{r_3},\vec{r_4}]}$ (Fig. 5.2(d)), which consists of

$$C_1, T_{a1}, T_{b1}, C_2, T_{a2}, T_{b2}, C_3, T_{a3}, T_{b3}, C_4, T_{a4}, T_{b4},$$

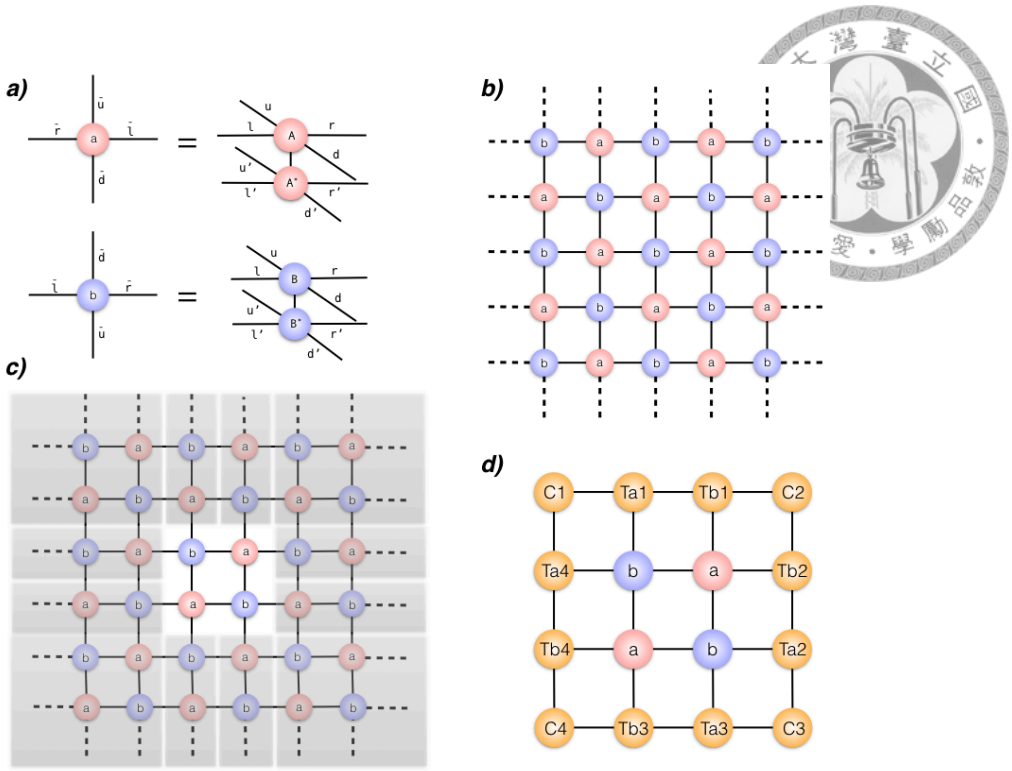

Figure 5.2: The red and blue tensor denotes on *odd* and *even* sites. The yellow one are time evolution operators $e^{-\tau H_{k,k+1}}$, $e^{-\tau H_{k+1,k}}$

For the approximation of environment, the directional variant of the CTMRG was developed. According to *directional coarse-graining moves*, the effective environment could be updated from four different moves , left, right, up and down and iterated until the environments converges.

For instance, the procedures to the left move, shown in the Fig. 5.3 which is derived by Roman and Vidal, is made up of four major steps,

1. Insertion: Insert two new columns which consist of $\{ T_{a1}, b, a, T_{b3} \}$ and $\{ T_{b1}, a, b, T_{a3} \}$ as in Fig. 5.3(b).

2. Absorption: In order to obtaining two new corner matrices $\tilde{C_1}$ and $\tilde{C_4}$, and two new transfer matrices $\tilde{T_{b4}}$ and $\tilde{T_{a4}}$, we contract tensors C_1 and T_{b1}, tensors C_3 and T_{a3}, tensors T_{a4} and b, and tensors T_{b4} and a. Then, contract tensors $\tilde{C_1}$ and $\tilde{T_{b4}}$, and tensors $\tilde{C_4}$ and $\tilde{T_{a4}}$, obtaining $\tilde{Q_1}$ and $\tilde{Q_4}$ which play significant rules for calculating isometries between $\tilde{T_{b4}}$ and $\tilde{T_{a4}}$ as in Fig. 5.3(c).

3. Renormalization: Truncate the vertical virtual bonds of $\widetilde{C_1}$, $\widetilde{T_{b4}}$, $\widetilde{T_{a4}}$, and $\widetilde{C_4}$ by contracting the isometries Z and W, where

$$Z^\dagger Z = I \tag{5.4}$$

$$W^\dagger W = I \tag{5.5}$$

and the renormalization of the left CTM, yield as

$$C_1' = Z^\dagger \tilde{C}_1 \tag{5.6}$$

$$T_{b4}' = Z\tilde{T}_{b4}W^\dagger \tag{5.7}$$

$$T_{a4}' = W\tilde{T}_{b4}Z^\dagger \tag{5.8}$$

$$C_4' = Z\widetilde{C_4} \tag{5.9}$$

See the Fig. 5.3(d) and 5.3(f).

4. Truncation: To determinate the isometries Z and W in the *renormalization* steps is the most significant part. In this case, we use the eigenvalue decomposition of

$$\tilde{C_1}\tilde{C_1^\dagger} + \tilde{C_4}\tilde{C_4^\dagger} = \tilde{Z}D_z\tilde{Z}^\dagger \tag{5.10}$$

$$\tilde{Q_1}\tilde{Q_1^\dagger} + \tilde{Q_4}\tilde{Q_4^\dagger} = \tilde{W}D_w\tilde{W}^\dagger \tag{5.11}$$

shown in Fig. 5.3(e). It's not hard to find that the the dimension of bonds of D_z and D_w increase to χ^2. For that reason, we have to truncate $\tilde{Z}$ and $\tilde{W}$ to isometries Z and W which are equivalent to keeping the columns of $\tilde{Z}$ and $\tilde{W}$ corresponding to χ largest eigenvalues of D_z and D_w.

Now, we need repeat the procedures in Fig. 5.3(b)-(d) again for absorbing the other inserted column in Fig. 5.3(d) and obtain a new effective environment $G'^{[\vec{r_1},\vec{r_2},\vec{r_3},\vec{r_4}]}$ for the four-site unit cell. By composing four variant moves of the CTM we build an epoch of CTMRG.

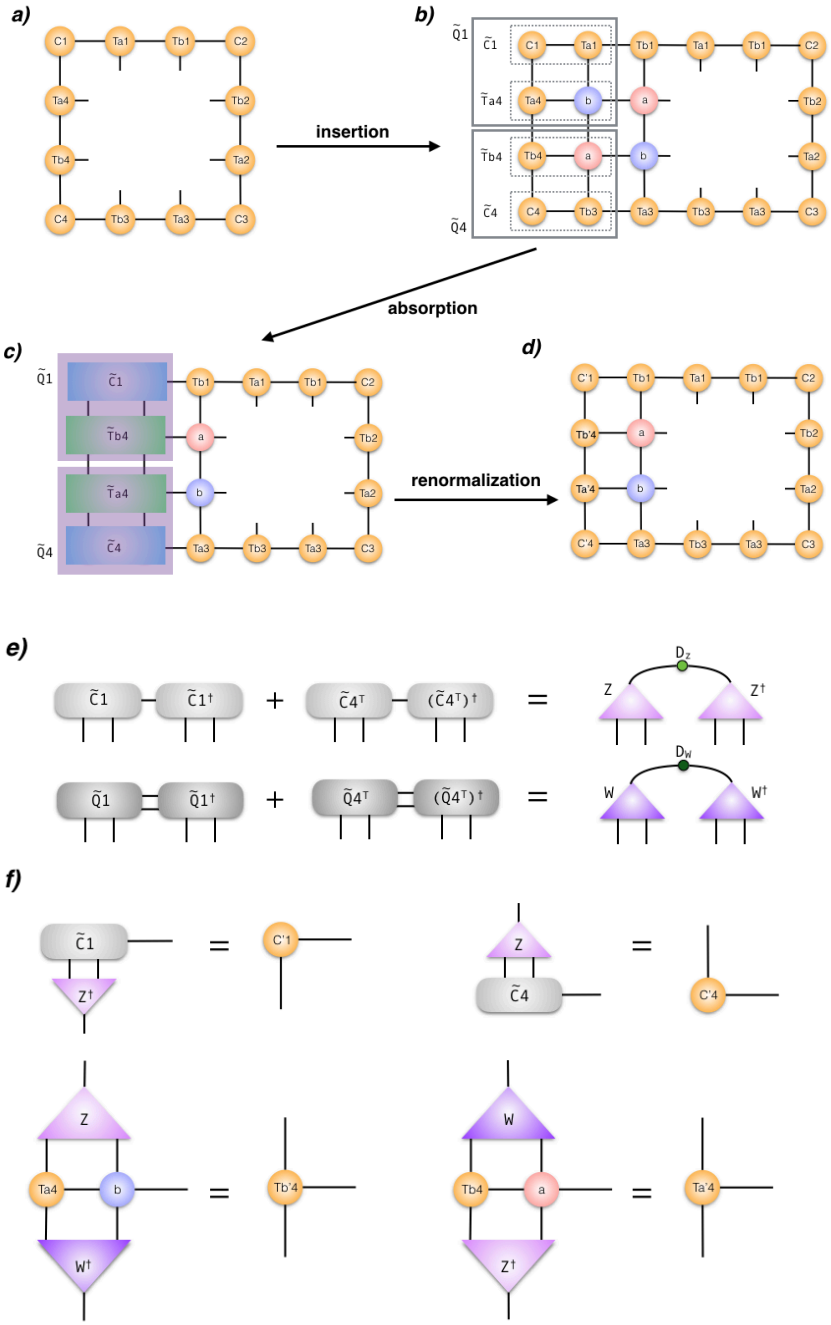

Figure 5.3: The red and blue tensor denotes on *odd* and *even* sites. The yellow one are time evolution operators $e^{-\tau H_{k,k+1}}$, $e^{-\tau H_{k+1,k}}$

5.2 Obtain States from PESS

CTM with PESS.

Chapter 6

Summary

Bibliography

[1] S. R. White, **69**, 2863 (1992).

[2] S. R. White, **48**, 10345 (1993).

[3] F. Verstraete and J. I. Cirac, **73**, 10.1103/PhysRevB.73.094423.

[4] S. Östlund and S. Rommer, **75**, 3537.

[5] V. Murg, F. Verstraete, and J. I. Cirac, **75**, 10.1103/PhysRevA.75.033605.

[6] F. Verstraete, V. Murg, and J. Cirac, **57**, 143.

[7] G. Vidal, **91** (2003), 10.1103/PhysRevLett.91.147902.

[8] G. Vidal, **93** (2004), 10.1103/PhysRevLett.93.040502.

[9] G. Vidal, **99** (2007), 10.1103/PhysRevLett.99.220405.

[10] J. Jordan, "Studies of infinite two-dimensional quantum lattice systems with projected entangled pair states," .

[11] R. Orús, **349**, 117.

[12] R. B. Bauer, "Tensor network states," .

[13] W. Li, J. von Delft, and T. Xiang, **86**, 10.1103/PhysRevB.86.195137.

[14] M. B. Hastings, **50**, 095207.

[15] G. Vidal, **98** (2007), 10.1103/PhysRevLett.98.070201.

[16] H. C. Jiang, Z. Y. Weng, and T. Xiang, **101**, 10.1103/PhysRevLett.101.090603.

[17] R. Orús and G. Vidal, **78**, 10.1103/PhysRevB.78.155117.